An Album of Fluid Motion

Assembled by Milton Van Dyke

Department of Mechanical Engineering

Stanford University, Stanford, California

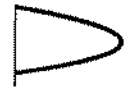

THE PARABOLIC PRESS

Stanford, California

1. Creeping Flow

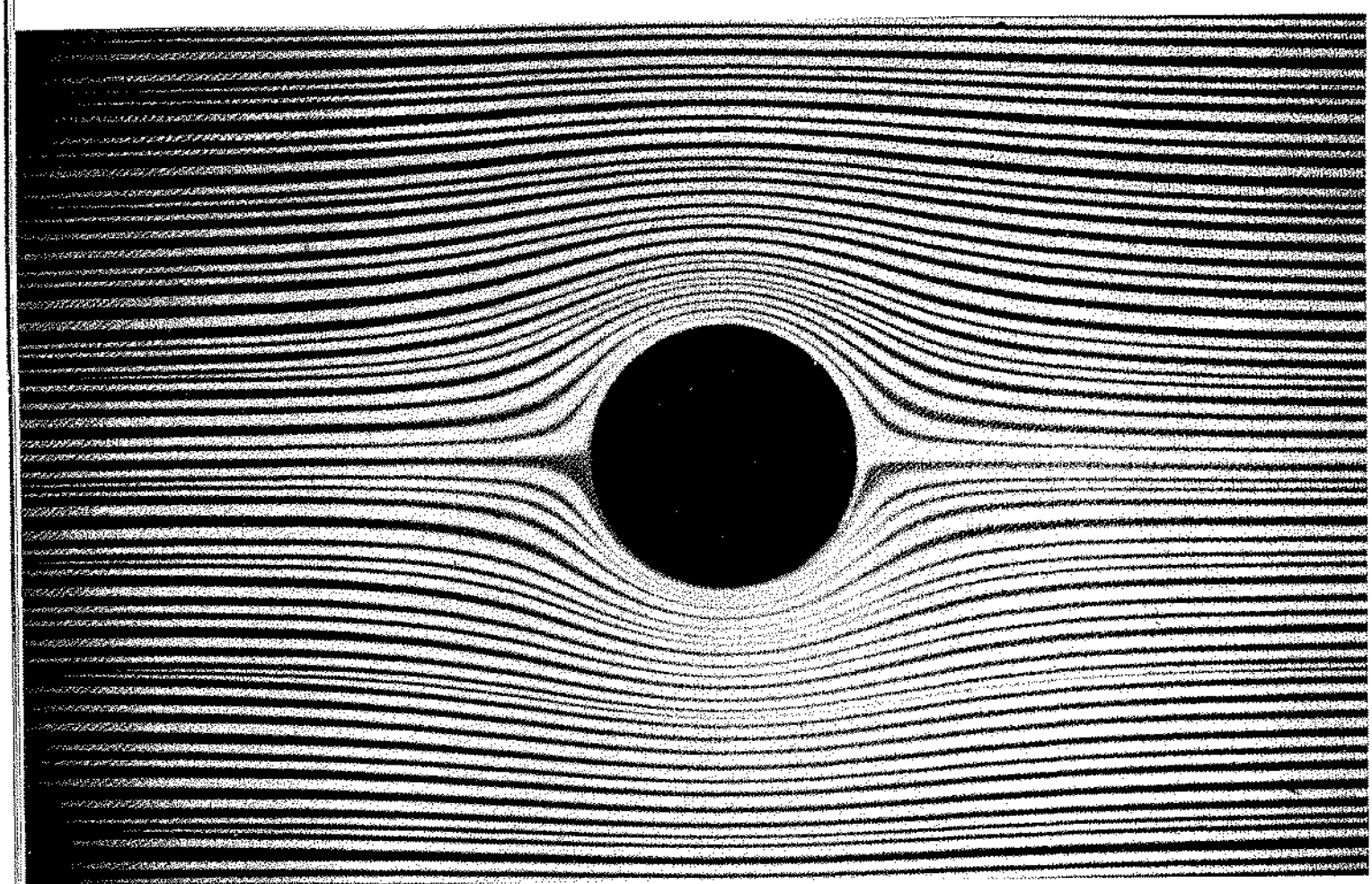

1. Hele-Shaw flow past a circle. Dye shows the streamlines in water flowing at 1 mm per second between glass plates spaced 1 mm apart. It is at first sight paradoxical that the best way of producing the unseparated pattern of plane potential flow past a bluff object, which would be spoiled by separation in a real fluid of even the slightest viscosity, is to go to the opposite extreme of creeping flow in a narrow gap, which is dominated by viscous forces. *Photograph by D. H. Peregrine*

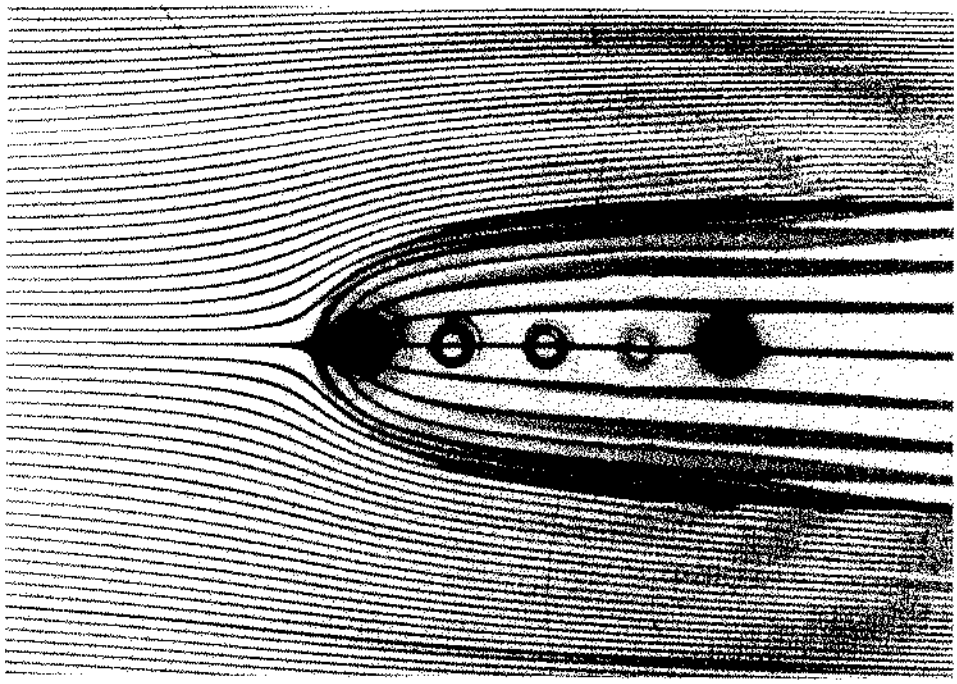

2. Hele-Shaw flow past a Rankine half-body. A viscous fluid is introduced through the orifice at the left into a uniform stream of the same fluid flowing between glass plates spaced 0.5 mm apart. Dye shows both the external and internal streamlines for plane potential flow past a semi-infinite body. The streamlines are slightly blurred because the rate of delivery of fluid to the source was changing as the photograph was made. *Taylor 1972*

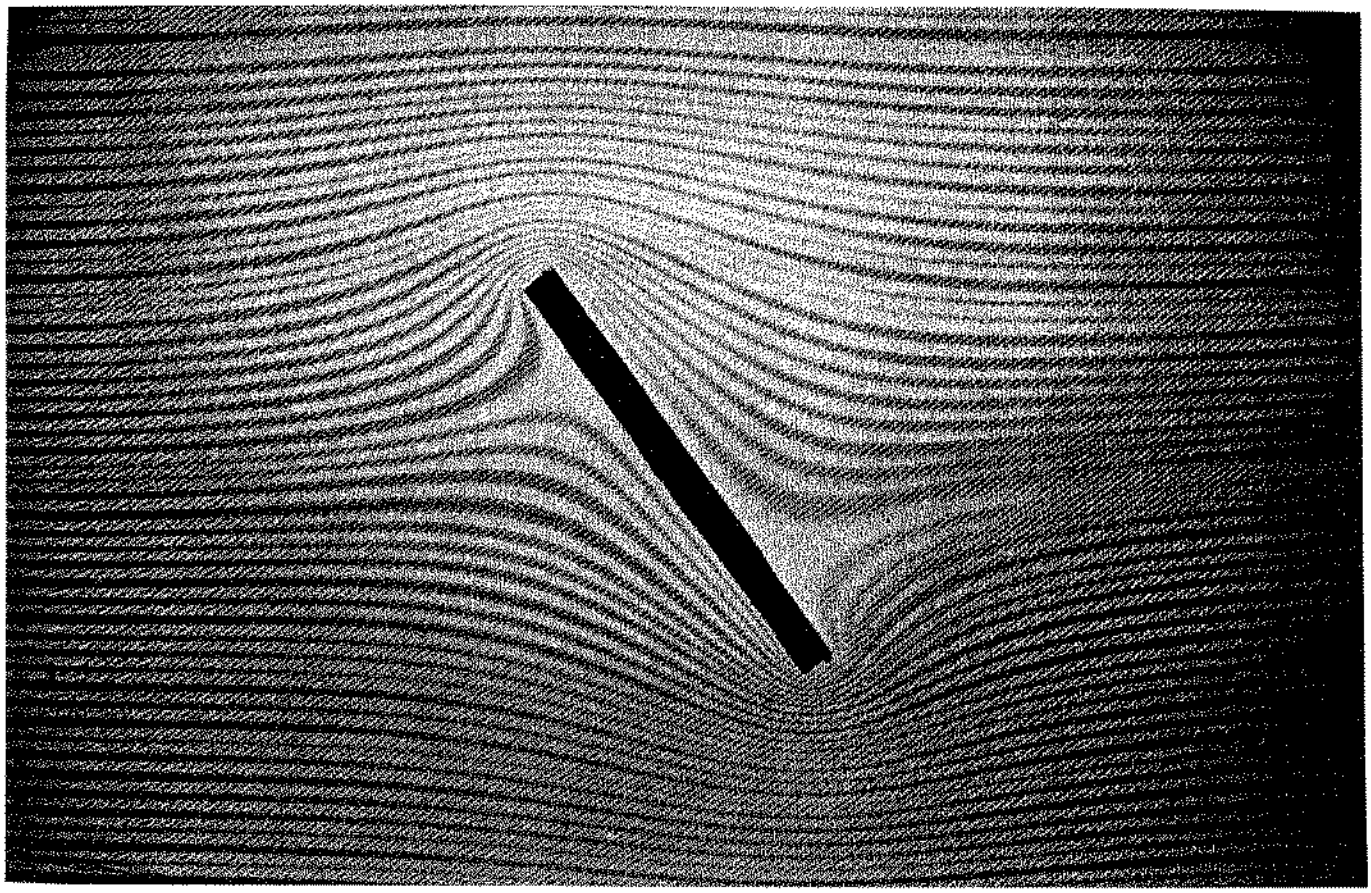

3. Hele-Shaw flow past an inclined plate. The Hele-Shaw analogy cannot represent a flow with circulation. It therefore shows the streamlines of potential flow past an inclined plate with zero lift. Dye flows in water between glass plates spaced 1 mm apart. *Photograph by D. H. Peregrine*

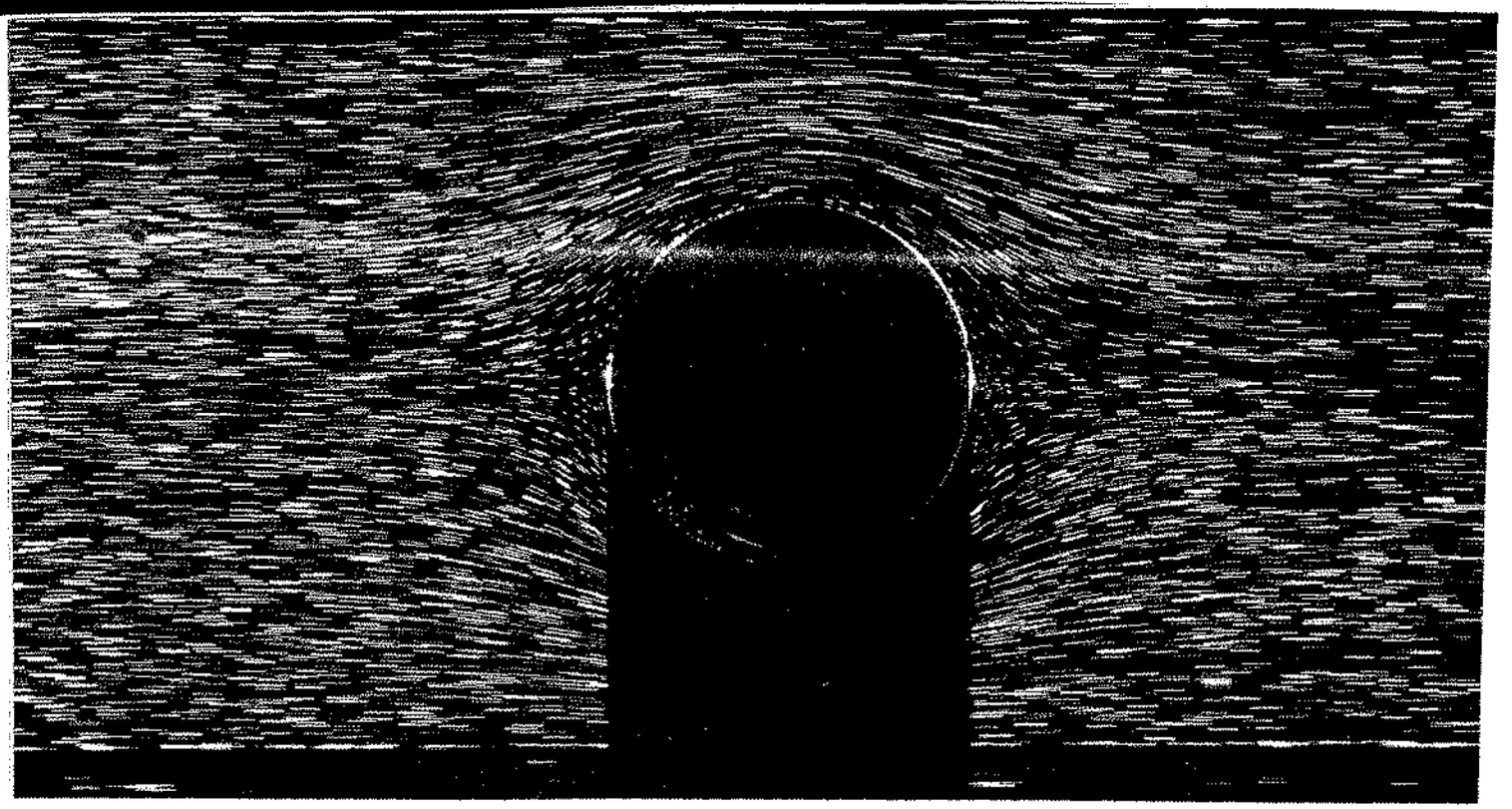

8. Sphere moving through a tube at $R=0.10$, relative motion. A free sphere is falling steadily down the axis of a tube of twice its diameter filled with glycerine. The camera is moved with the speed of the sphere to show the flow relative to it. The photograph has been rotated to show flo from left to right. Tiny magnesium cuttings are illuminate by a thin sheet of light, which casts a shadow of th sphere. *Coutanceau 1968*

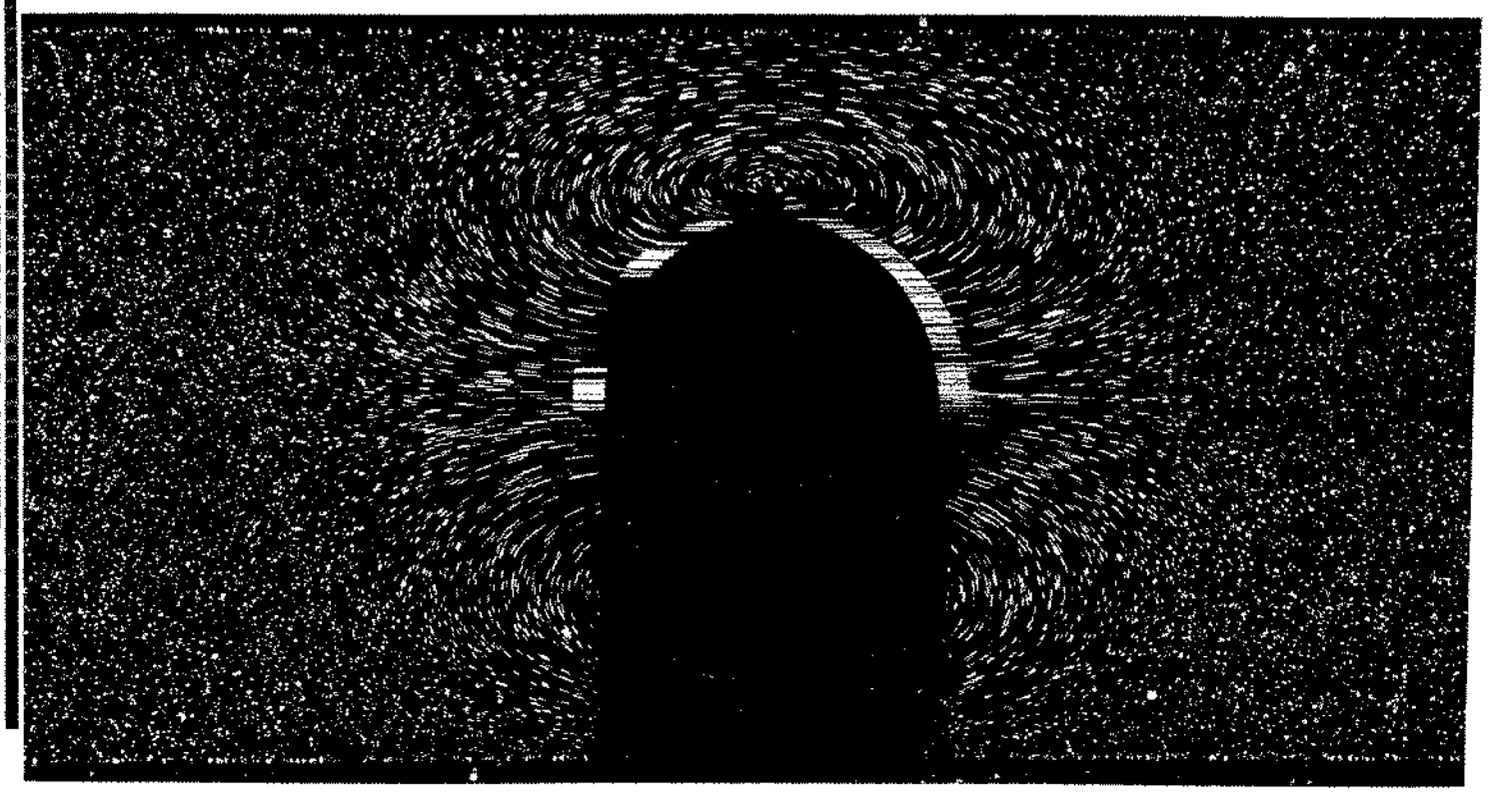

9. Sphere moving through a tube at $R=0.10$, absolute motion. In contrast to the photograph above, here the camera remains fixed with respect to the distant fluid. During the exposure the sphere has moved from left to right less than a tenth of a diameter, to show the absolute m tion of the fluid. At this small Reynolds number the fl pattern, shown by magnesium cuttings in oil, looks co pletely symmetric fore-and-aft. *Coutanceau 1968*

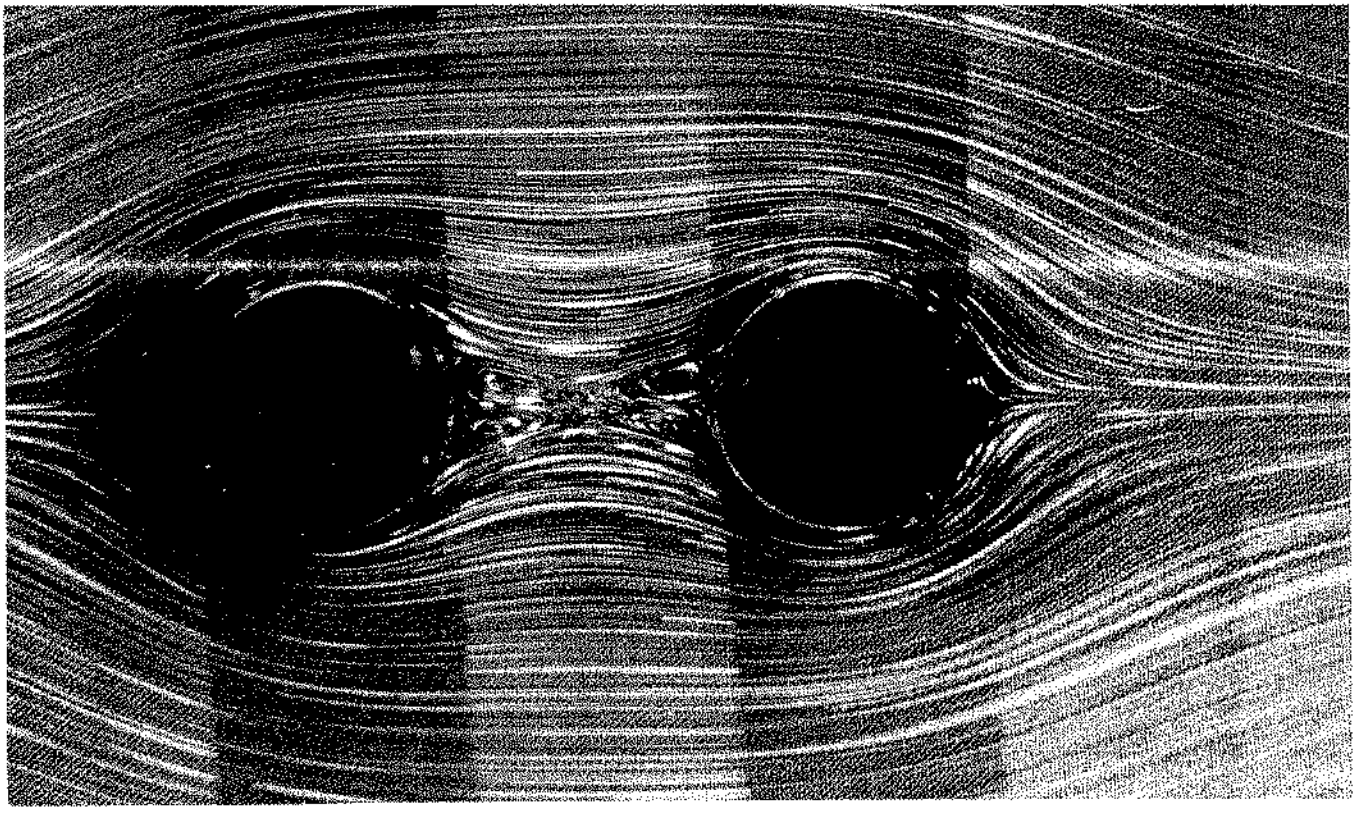

15. Creeping flow past two circles in tandem. The gap is one diameter, and the Reynolds number is 0.01. Streamlines are shown by aluminum dust in glycerine. The interaction produces separation at any speed, whereas flow past an isolated circular cylinder separates only above a Reynolds number of 5. *Taneda 1979*

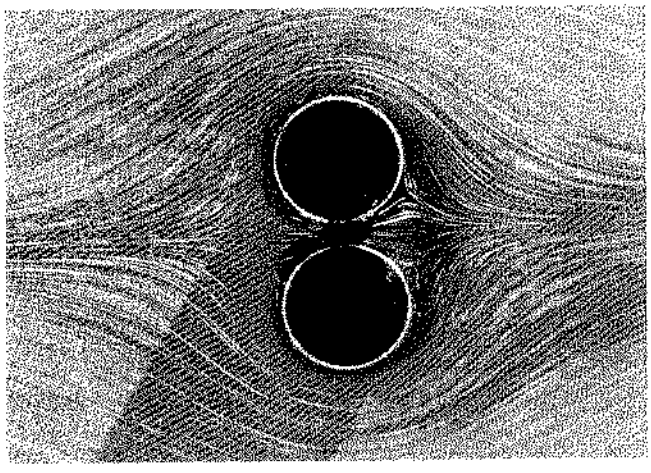

16. Creeping flow past two circles side-by-side. The Reynolds number is 0.01, and the gap between the cylinders is 0.2 of their diameter. Aluminum dust in glycerine shows that there is no-apparent separation. *Taneda 1979*

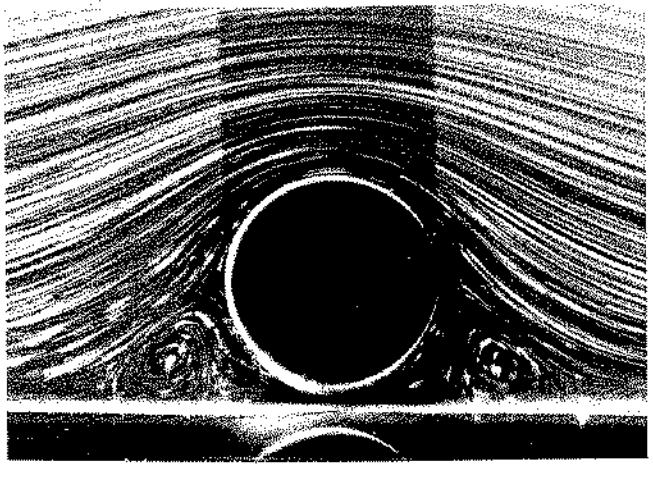

17. Circle in slow linear shear near a plate. The cylinder is 0.1 diameter from the plate, or 0.2 diameter from its hydrodynamic image, which is actually visible as an optical image. The Reynolds number is 0.01 based on the shear rate. Large recirculating eddies form because the glycerine must stick to the plate, in contrast to the photograph above, where it flows along the symmetry plane. *Taneda 1979*

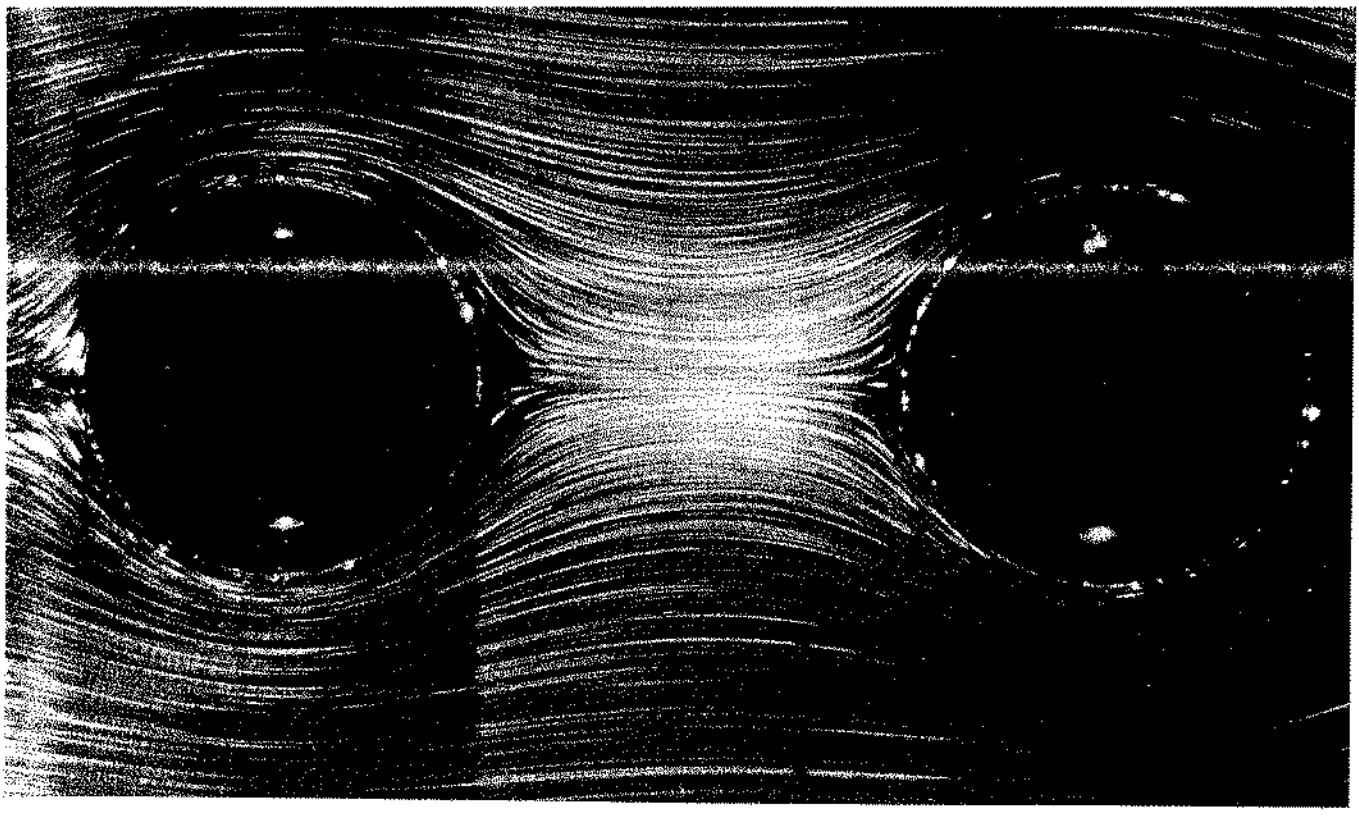

18. Creeping flow past two spheres in tandem. With the same spacing and approximately the same Reynolds number as the circles opposite, spheres show no sign of separation. This is consistent with the fact that separation on an isolated sphere appears only above a Reynolds number of 20, compared with 5 for a circle. Aluminum dust is illuminated in glycerine. *Taneda 1979*

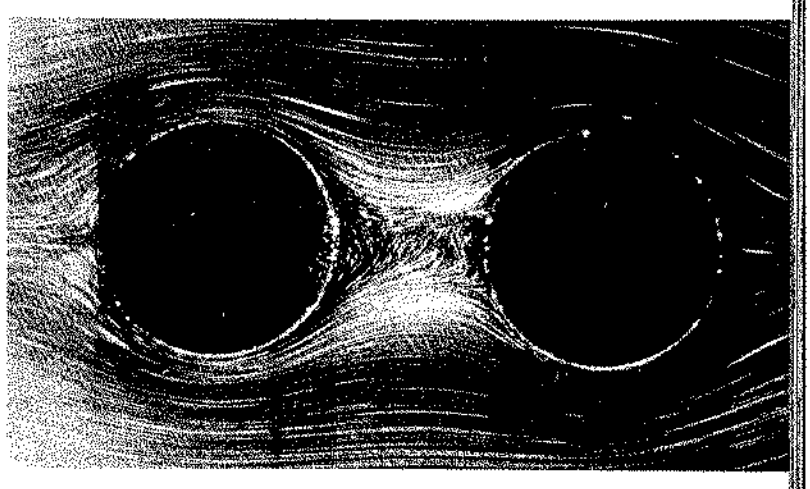

19. Creeping flow past closer spheres. At a spacing of 0.7 diameter, spheres in tandem show separation much like that between the circles spaced one diameter in figure 15. The diameter is 1.6 cm, and the Reynolds number 0.013. *Taneda 1979*

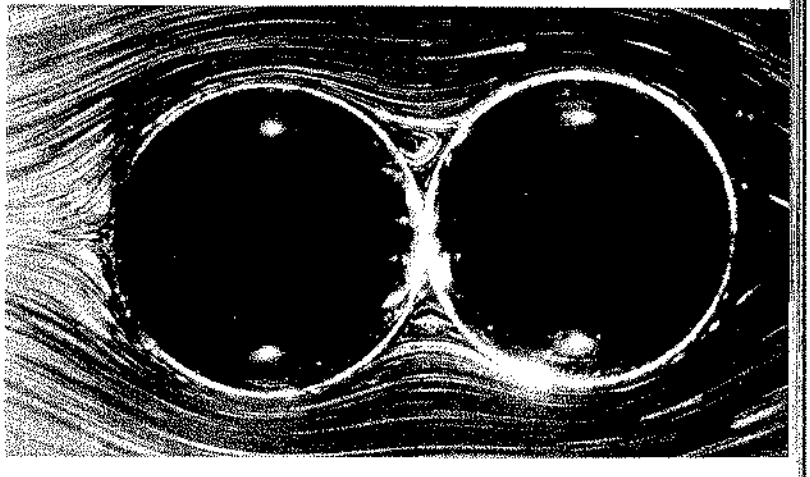

20. Creeping flow past tangent spheres. At the same Reynolds number of 0.013 the two pairs of vortex rings above have now merged into a single pair. Theory predicts, much as for the wedge in figure 10, an infinite sequence of vortex rings nested toward the contact point. *Taneda 1979*

2. Laminar Flow

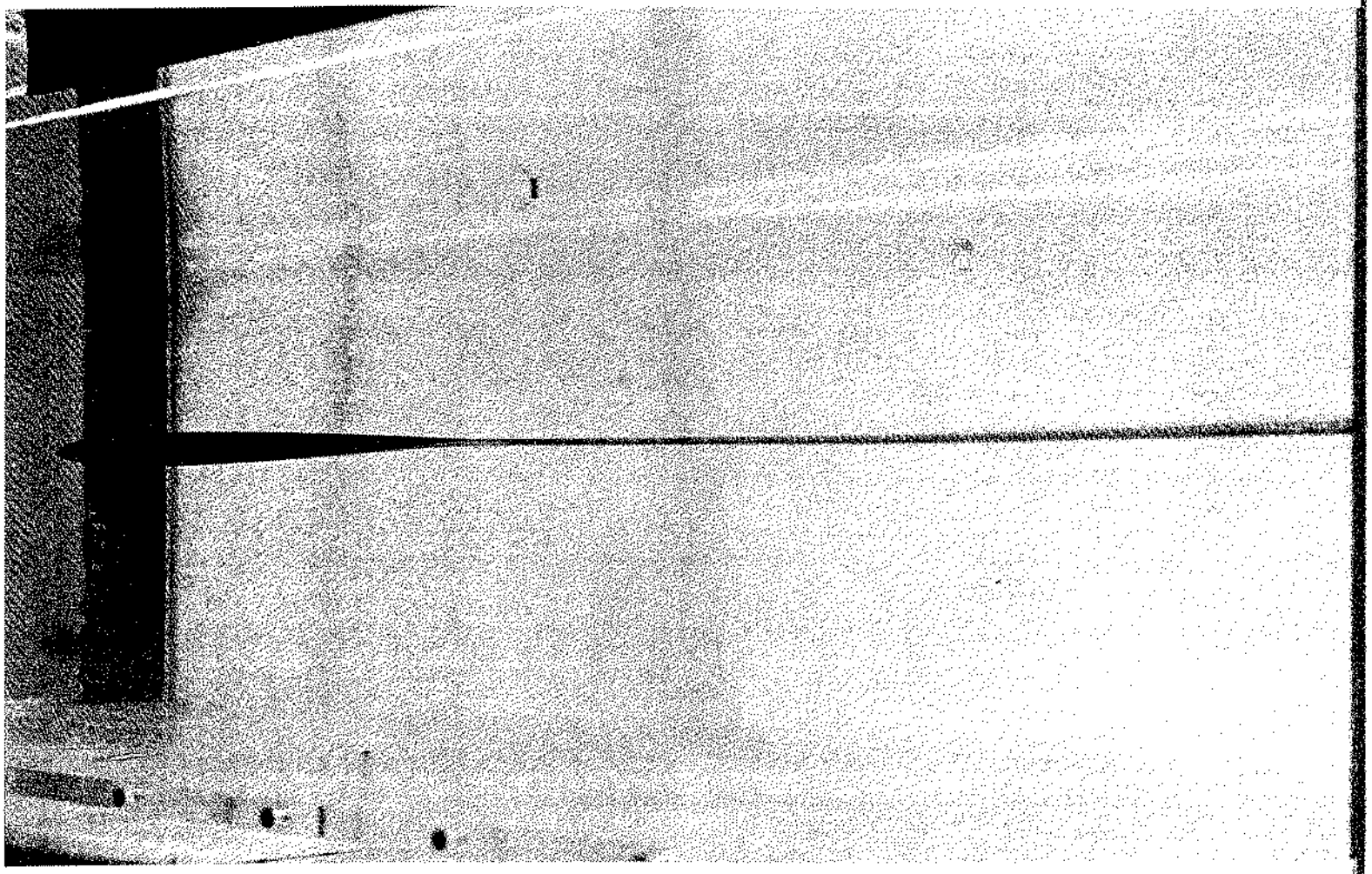

21. Laminar wake of a slender body of revolution. A sharp-tailed slender body of revolution is supported by fine tungsten wires and accurately aligned with the free stream in a water tunnel. The Reynolds number is 3600 based on maximum diameter. Dye released into the boundary layer shows the core of the wake, which remains laminar to the limit of this photograph. Varicose instability and transition to turbulence occur farther downstream. *Photograph by Francis Hama*

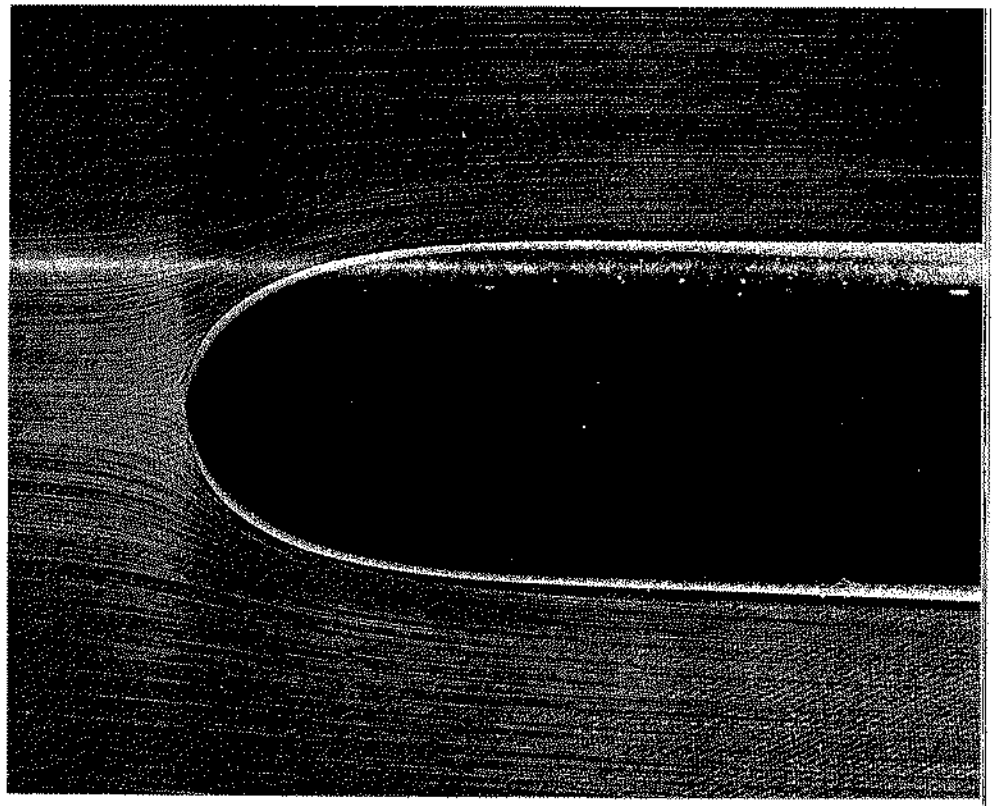

22. Axisymmetric flow past a Rankine ogive. This is the body of revolution that would be produced by a point potential source in a uniform stream—the axisymmetric counterpart of the plane half-body of figure 2. Its shape is so gentle that at zero incidence and a Reynolds number of 6000 based on diameter the flow remains attached and laminar. Streamlines are made visible by tiny air bubbles in water, illuminated by a sheet of light in the mid-plane. *ONERA photograph, Werlé 1962*

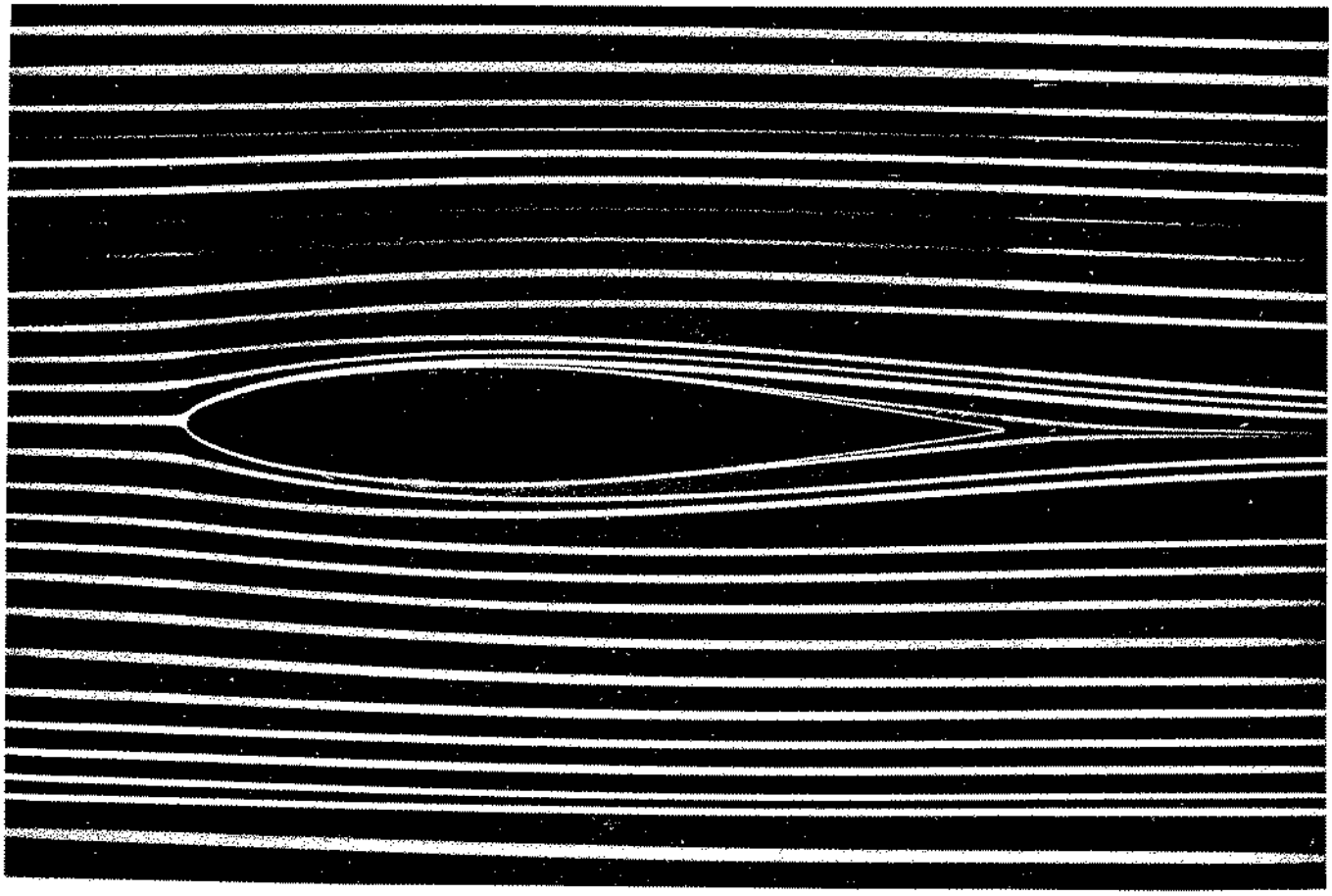

23. Symmetric plane flow past an airfoil. An NACA 64A015 profile is at zero incidence in a water tunnel. The Reynolds number is 7000 based on the chordlength. Streamlines are shown by colored fluid introduced upstream. The flow is evidently laminar and appears to be unseparated, though one might anticipate a small separated region near the trailing edge. *ONERA photograph, Werlé 1974*

24. Circular cylinder at $R=1.54$. At this Reynolds number the streamline pattern has clearly lost the fore-and-aft symmetry of figure 6. However, the flow has not yet separated at the rear. That begins at about $R=5$, though the value is not known accurately. Streamlines are made visible by aluminum powder in water. *Photograph by Sadatoshi Taneda*

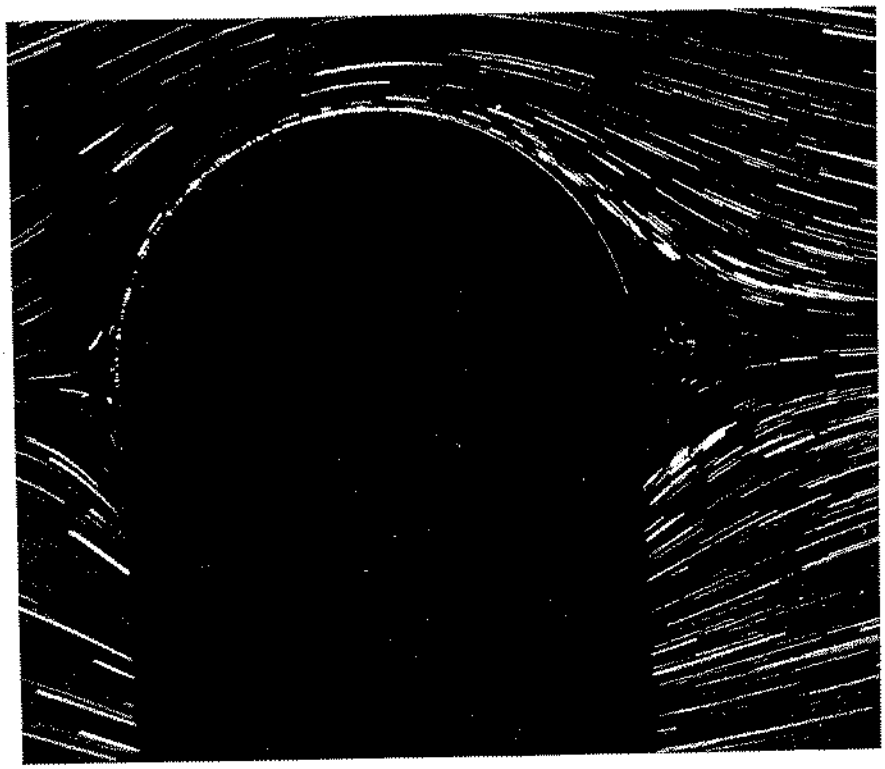

25. Sphere at $R=9.8$. Here too, with wall effects negligible, the streamline pattern is distinctly asymmetric, in contrast to the creeping flow of figure 8. The fluid is evidently moving very slowly at the rear, making it difficult to estimate the onset of separation. The flow is presumably attached here, because separation is believed to begin above $R=20$. Streamlines are shown by magnesium cuttings illuminated in water. *Photograph by Madeleine Coutanceau and Michele Payard*

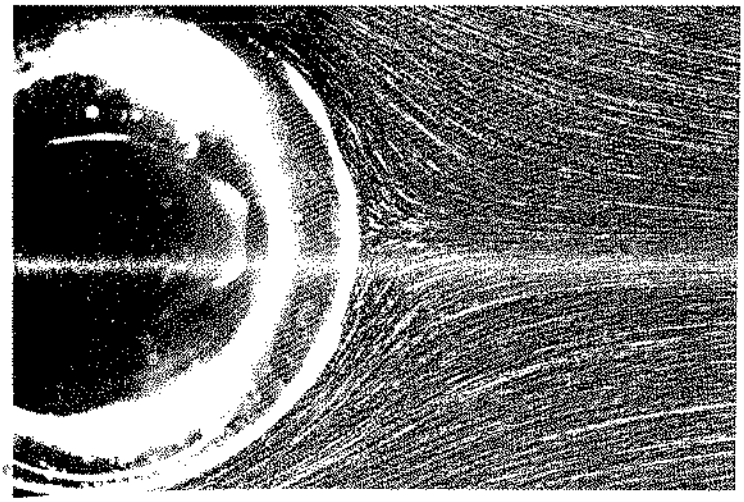

26. Flow behind a sphere at $R=8.15$. A steel ball bearing supported laterally on a fine piano wire is towed through water containing suspended aluminum dust, and illuminated by a sheet of light in the equatorial plane. The flow is clearly not yet separated. *Photograph by Sadatoshi Taneda*

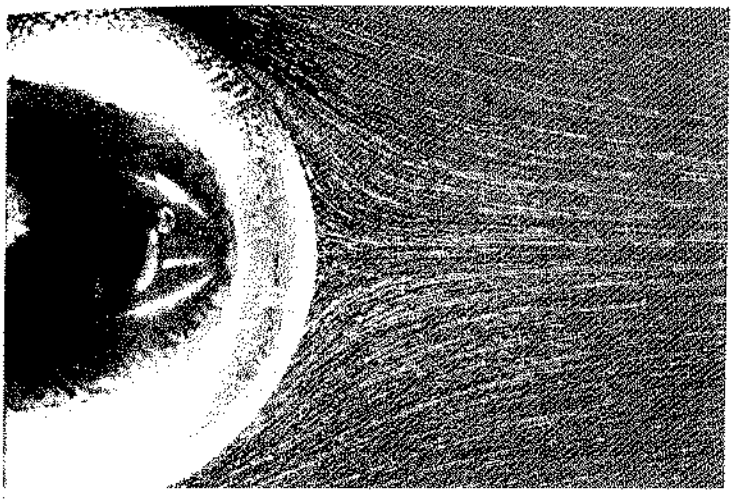

27. Flow behind a sphere at $R=17.9$. As the speed increases it is difficult to discern the onset of separation at the rearmost point. Here the flow must still be attached, because these experiments have indicated that separation behind an isolated sphere begins at about $R=24$. *Taneda 1956b*

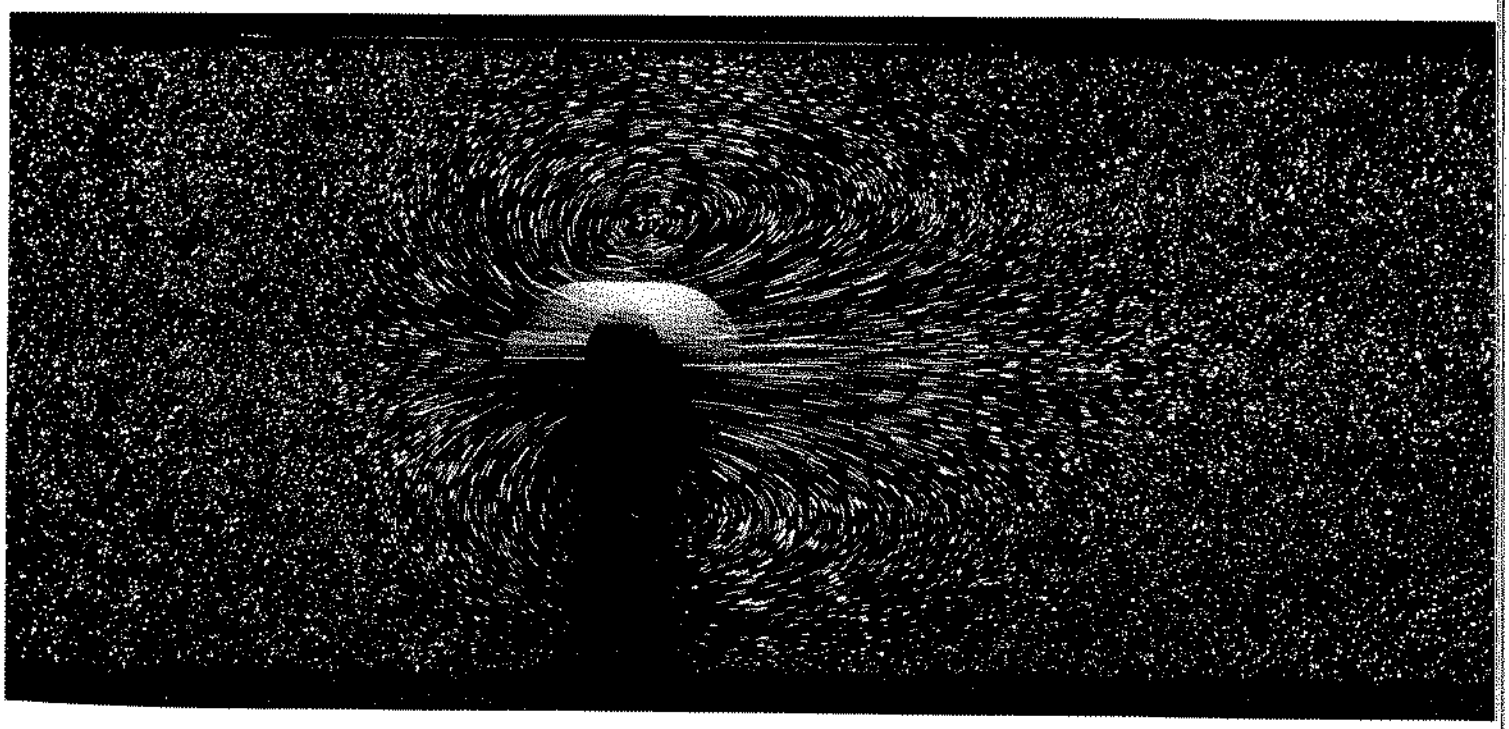

28. Sphere moving through a tube at $R=6.9$, absolute motion. The sphere is one-fourth the diameter of the tube. It has moved to the left through one radius. In contrast to the creeping motion of figure 9, there is at this modest Reynolds number the beginning of a wake: the disturbances extend considerably farther behind the sphere than ahead. Magnesium cuttings are illuminated in silicone oil. *Archives de l'Académie des Sciences de Paris. Coutanceau 1972*

3. Separation

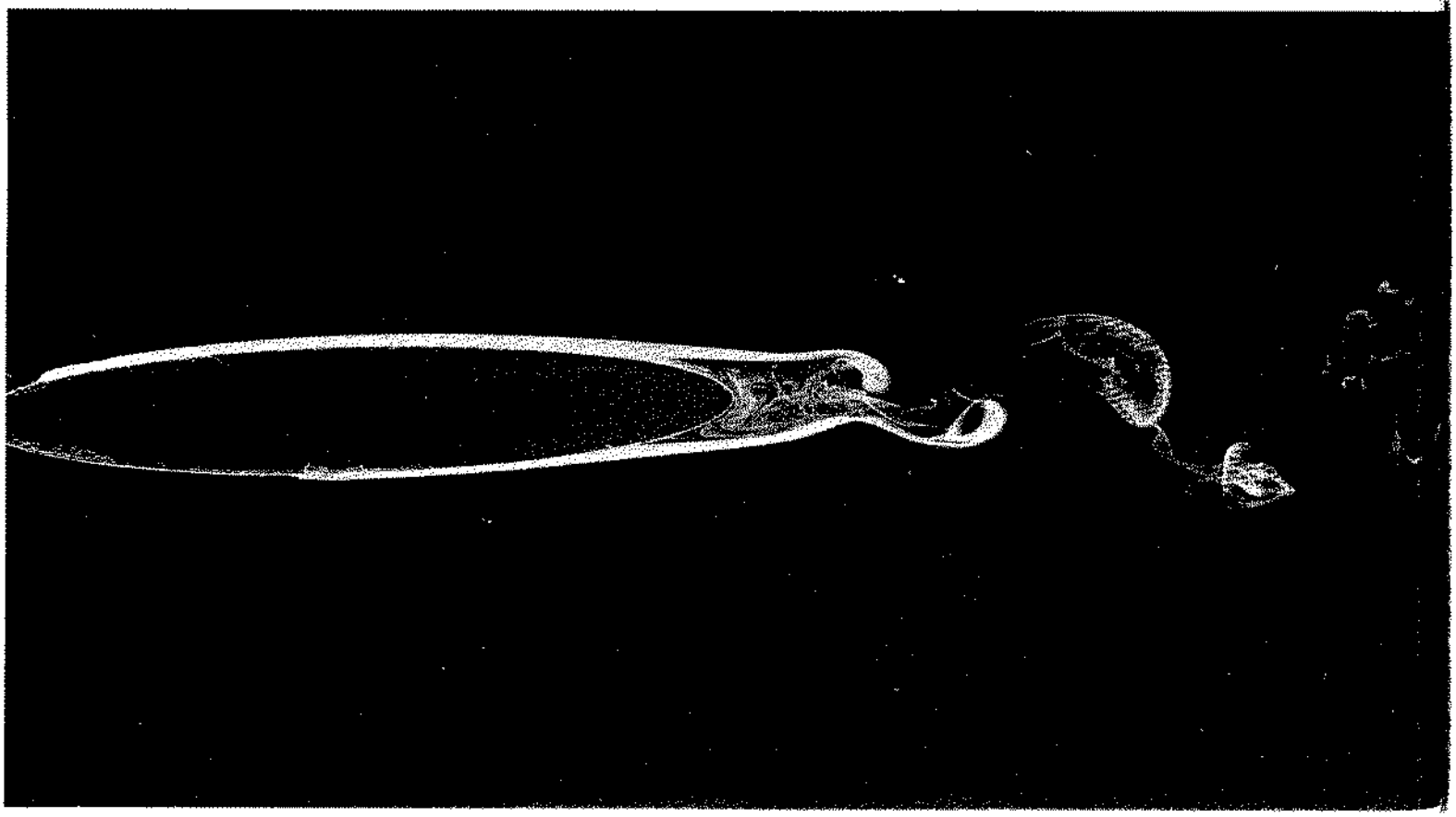

32. Laminar separation on a thin ellipse. A 6:1 elliptic cylinder is held at zero angle of attack in a wind tunnel. The Reynolds number is 4000 based on chord. Drops of titanium tetrachloride on the surface form white smoke, which shows the laminar boundary layer separating at the rear. *Bradshaw 1970*

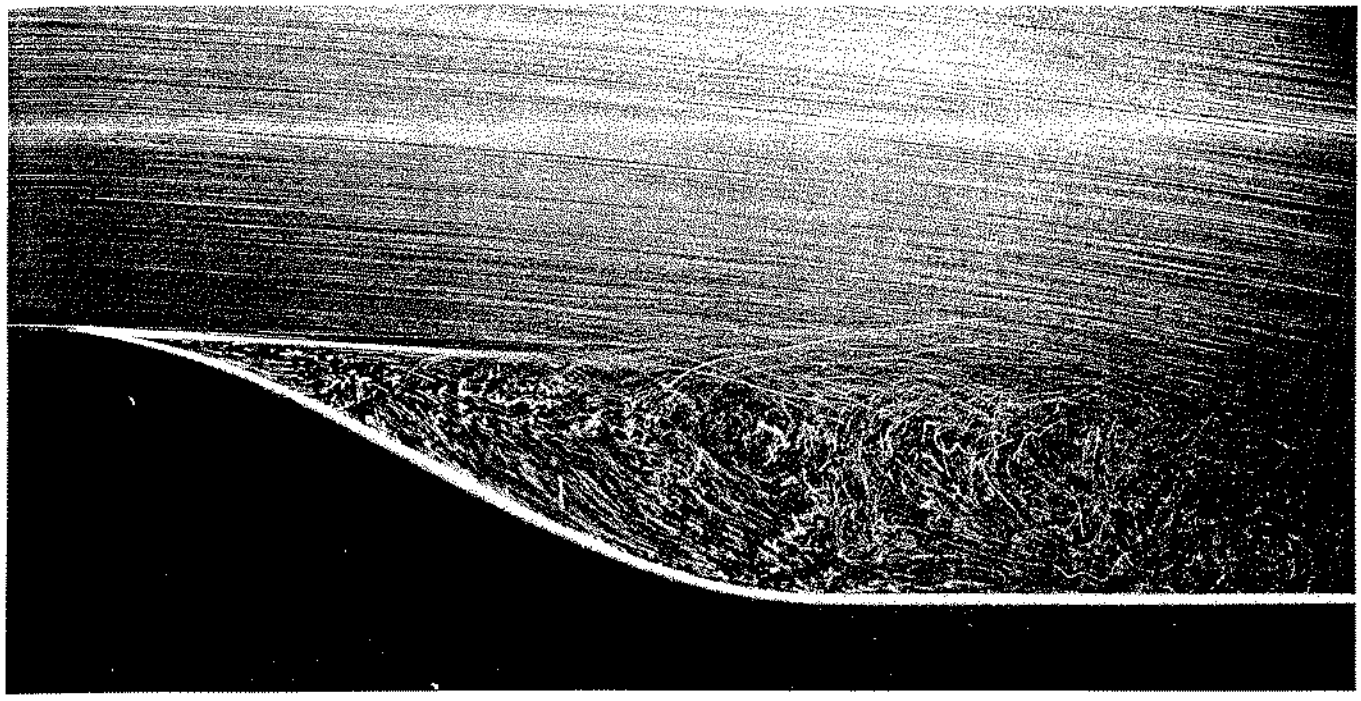

38. Laminar separation from a curved wall. Air bubbles in water show the separation of a laminar boundary layer whose Reynolds number is 20,000 based on distance from the leading edge (not shown). Because it is free of bubbles, the boundary layer appears as a thin dark line at the left. It separates tangentially near the start of the convex surface, remaining laminar for the distance to which the dark line persists, and then becomes unstable and turbulent. *ONERA photograph, Werlé 1974*

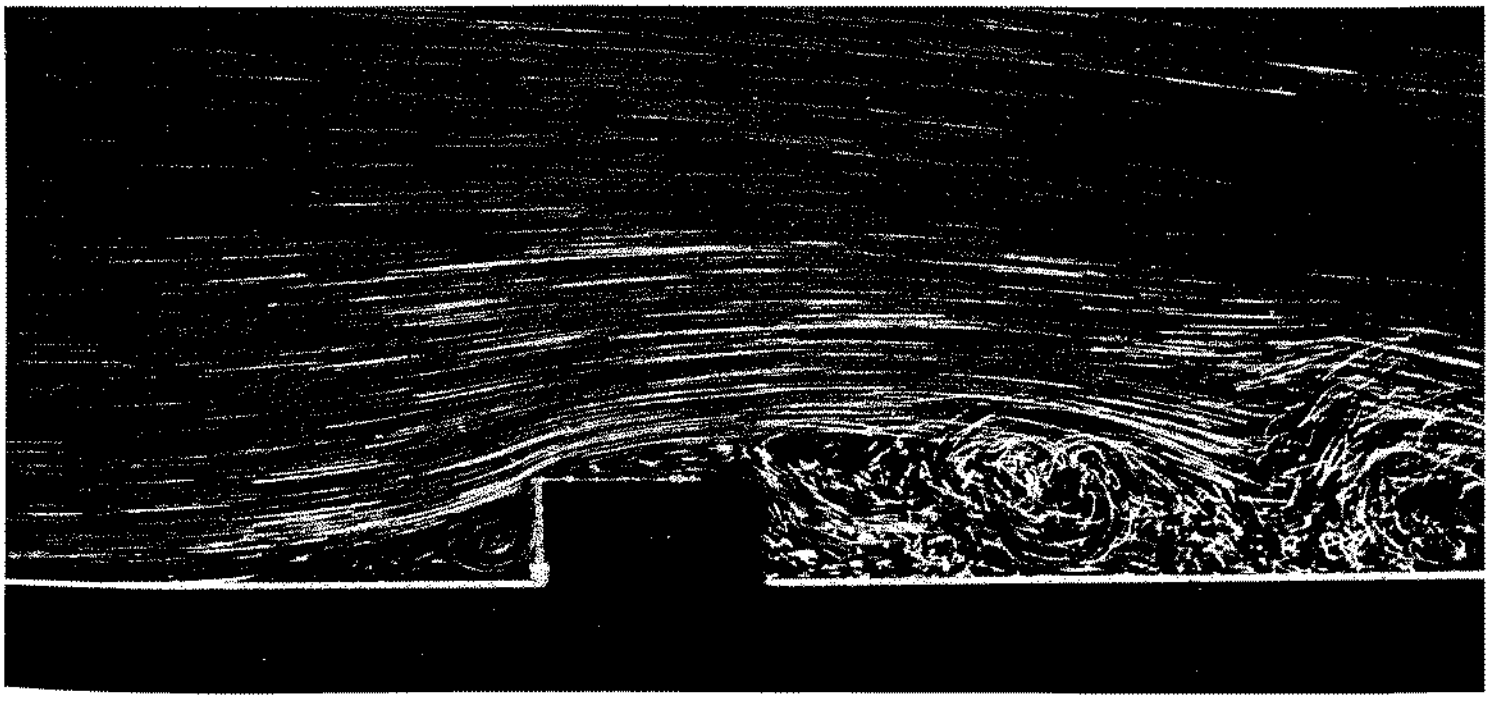

39. Turbulent separation over a rectangular block on a plate. The step height is large compared with the thickness of the oncoming laminar boundary layer. The flow is effectively plane, so that the recirculating region ahead of the step is closed, whereas in the corresponding three-dimensional flow of figure 92 it is open and drains around the sides. *ONERA photograph, Werlé 1974*

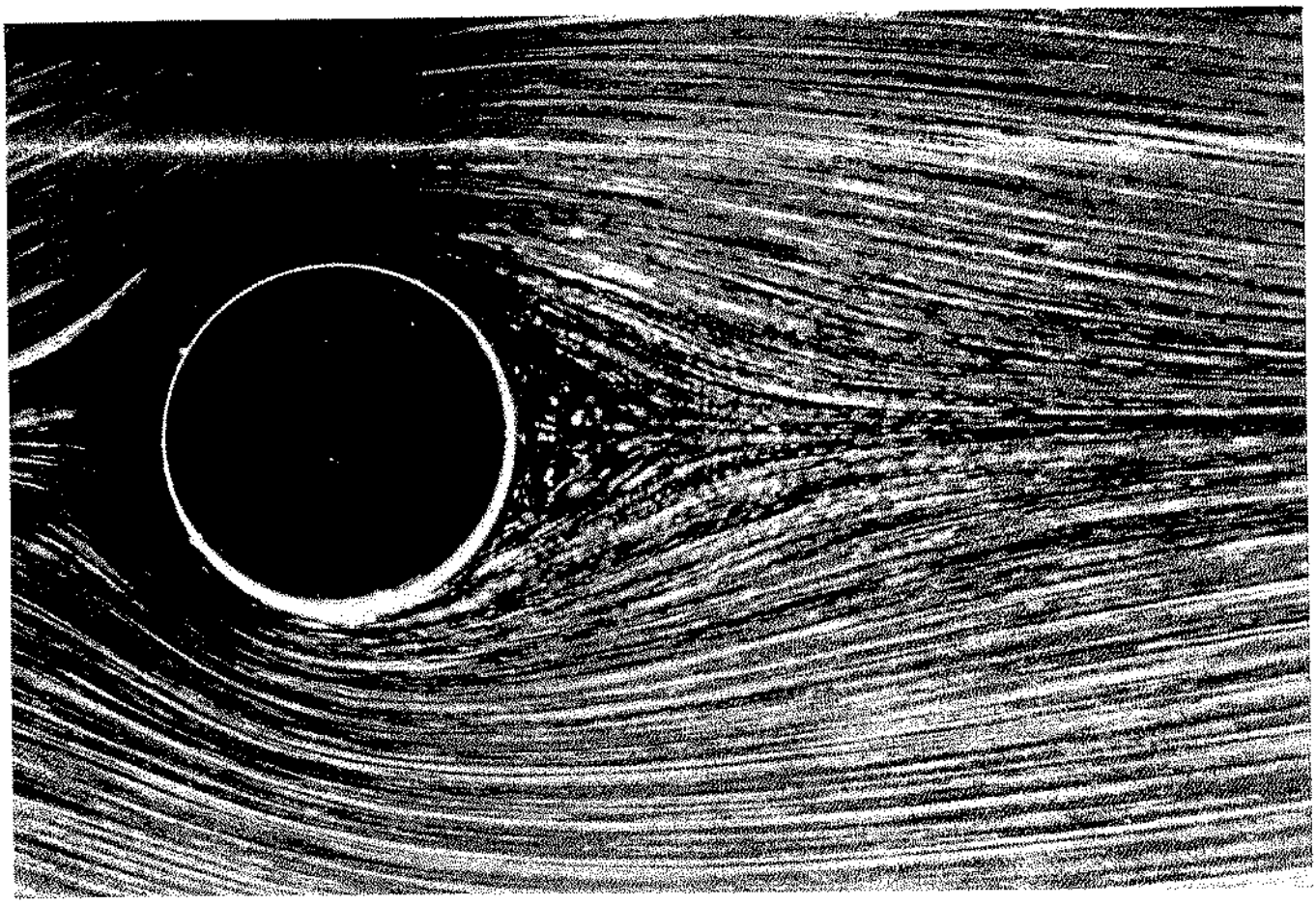

40. Circular cylinder at $R=9.6$. Here, in contrast to figure 24, the flow has clearly separated to form a pair of recirculating eddies. The cylinder is moving through a tank of water containing aluminum powder, and is illuminated by a sheet of light below the free surface. Extrapolation of such experiments to unbounded flow suggests separation at $R=4$ or 5, whereas most numerical computations give $R=5$ to 7. *Photograph by Sadatoshi Taneda*

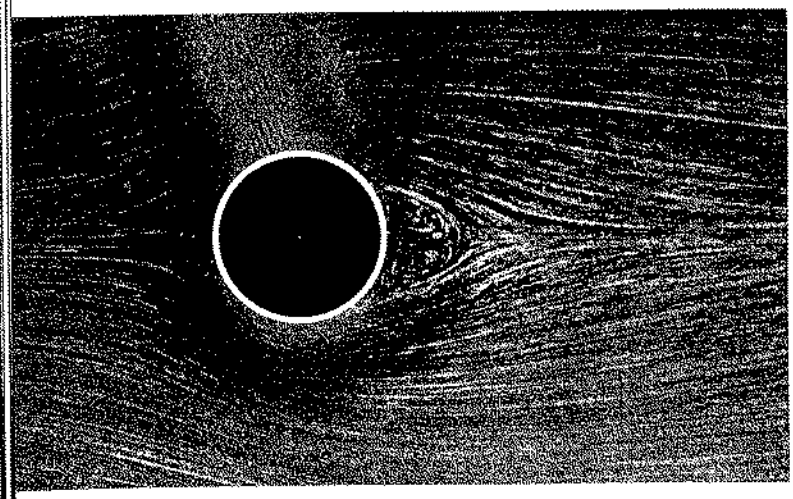

41. Circular cylinder at $R=13.1$. The standing eddies become elongated in the flow direction as the speed increases. Their length is found to increase linearly with Reynolds number until the flow becomes unstable above $R=40$. *Taneda 1956a*

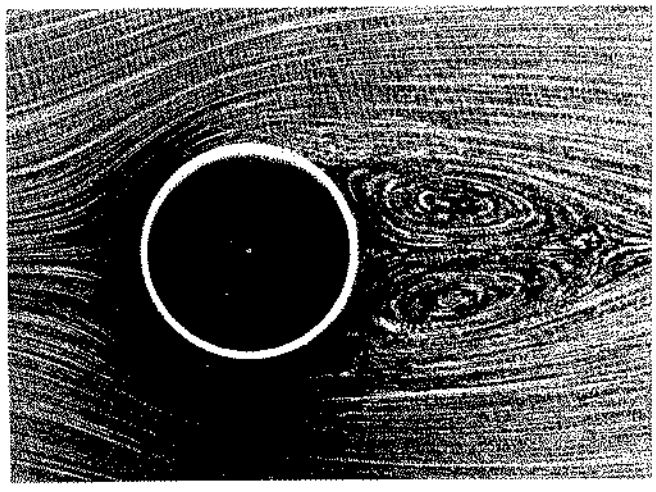

42. Circular cylinder at $R=26$. The downstream distance to the cores of the eddies also increases linearly with Reynolds number. However, the lateral distance between the cores appears to grow more nearly as the square root. *Photograph by Sadatoshi Taneda*

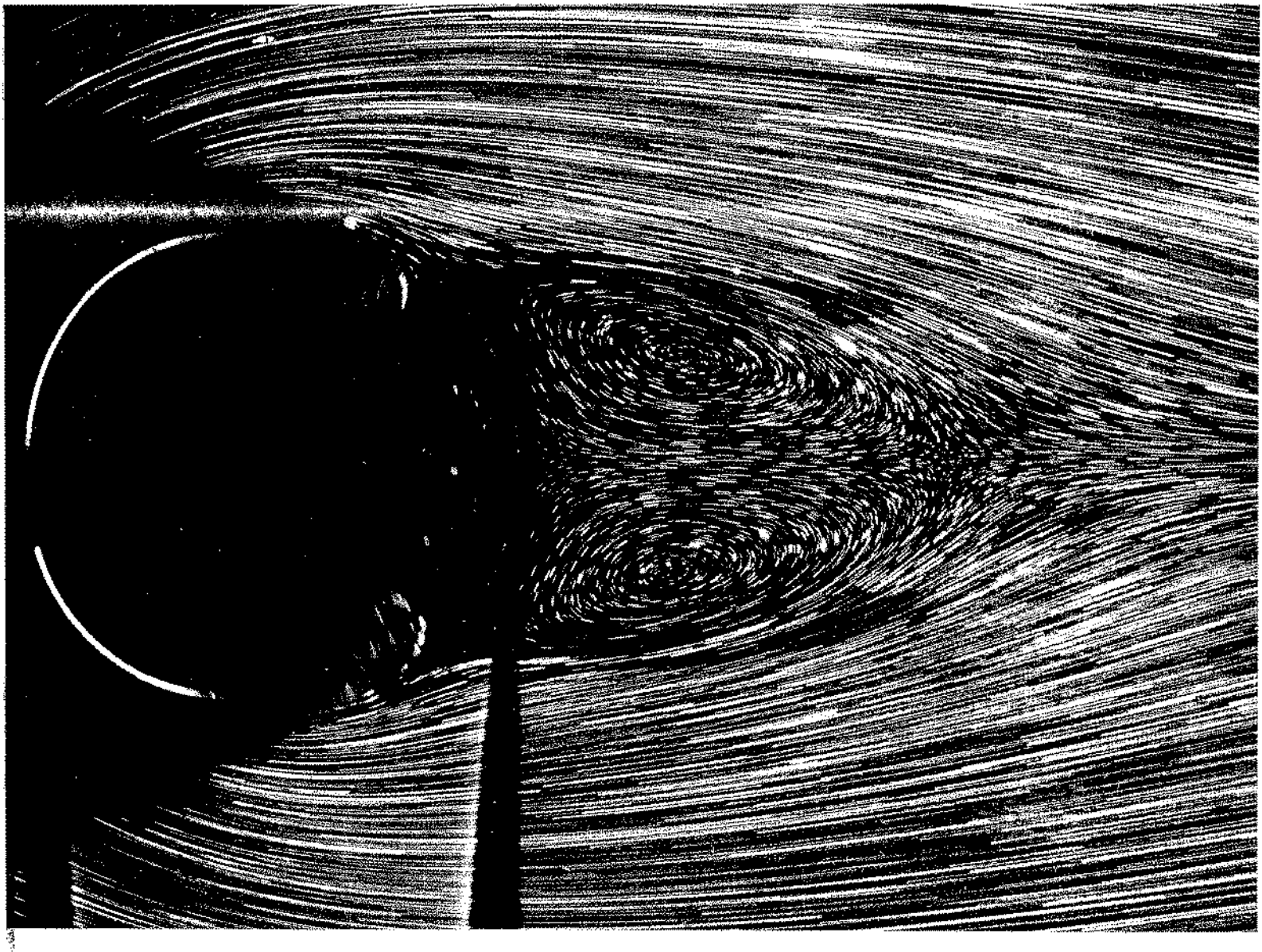

43. Circular cylinder at $R=24.3$. A different view of the flow is obtained by moving a cylinder through oil. Tiny magnesium cuttings are illuminated by a sheet of light from an arc projector. The two dark wedges below the circle are an optical effect. The lengths of the particle trajectories have been measured to find the velocity field to within two per cent. *Coutanceau & Bouard 1977*

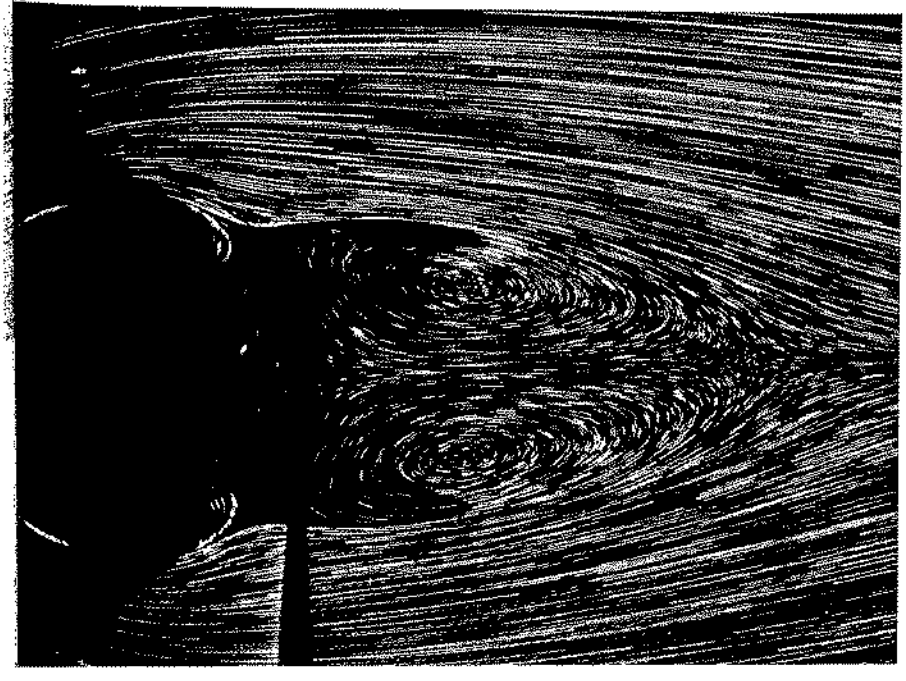

44. Circular cylinder at $R=30.2$. The flow is here still completely steady with the recirculating wake more than one diameter long. The walls of the tank, 8 diameters away, have little effect at these speeds. *Photograph by Madeleine Coutanceau and Roger Bouard*

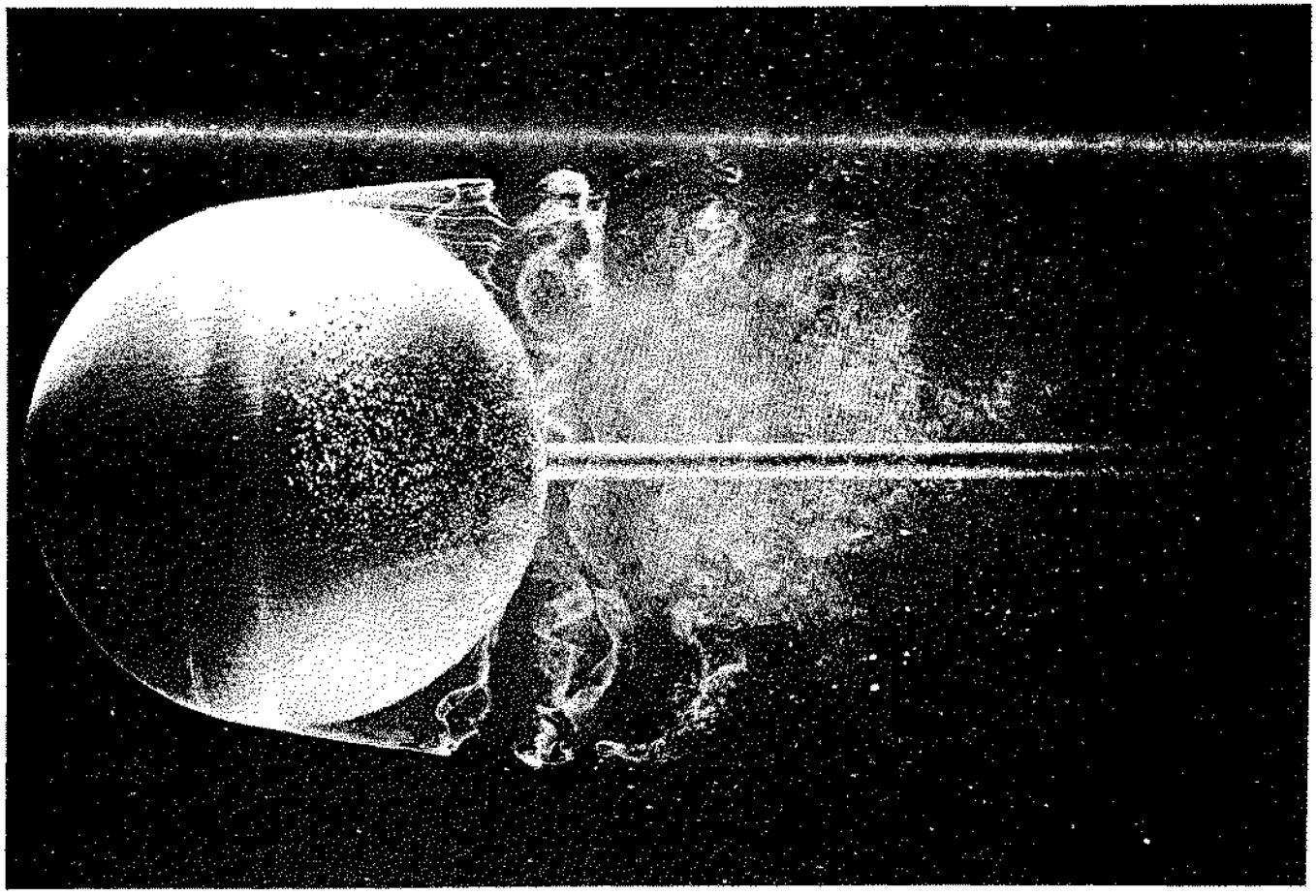

55. Instantaneous flow past a sphere at R=15,000. Dye in water shows a laminar boundary layer separating ahead of the equator and remaining laminar for almost one radius. It then becomes unstable and quickly turns turbulent. *ONERA photograph, Werlé 1980*

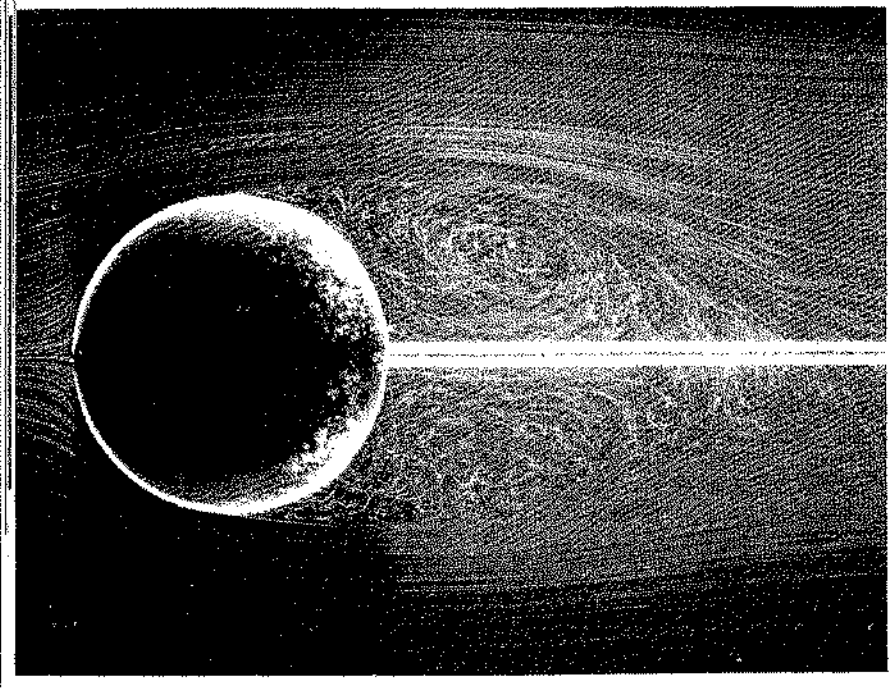

56. Mean flow past a sphere at R=15,000. A time exposure of air bubbles in water shows an averaged streamline pattern in the meridian plane for the flow that was photographed instantaneously above. *ONERA photograph by Henri Werlé*

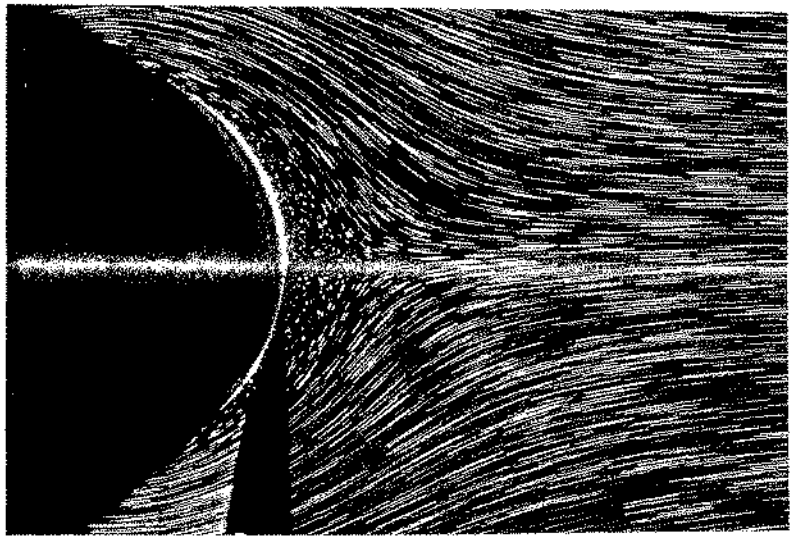

$R=50,\ Ut/d=0.5$

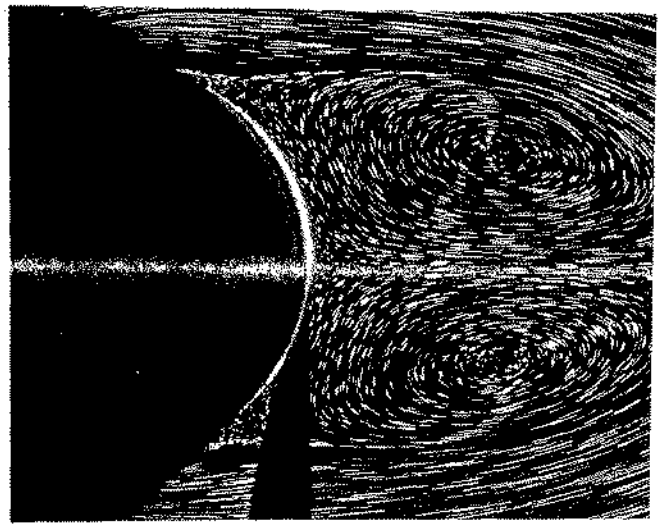

$R=50,\ Ut/d=2.5$

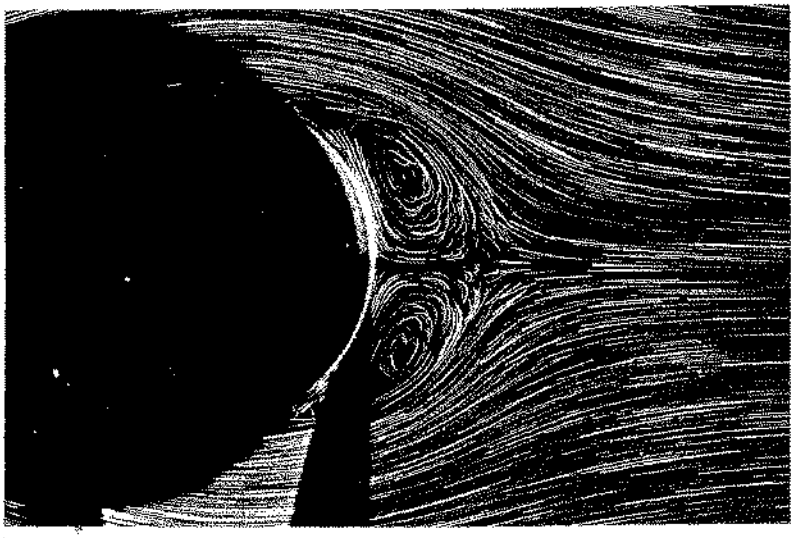

$R=500,\ Ut/d=1.0$

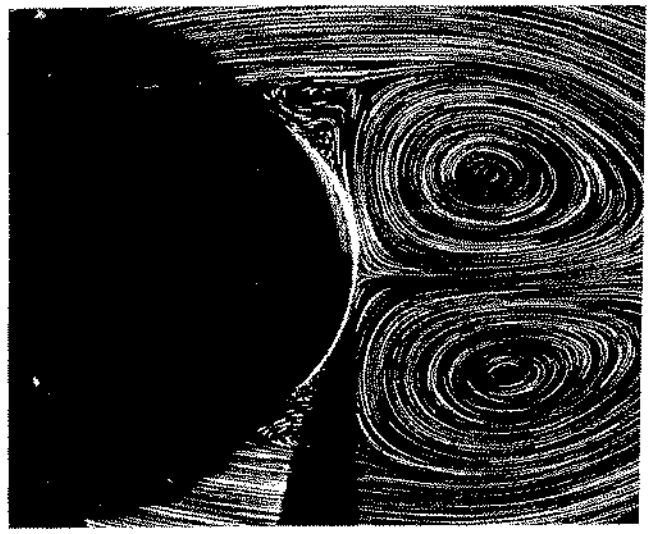

$R=500,\ Ut/d=3.0$

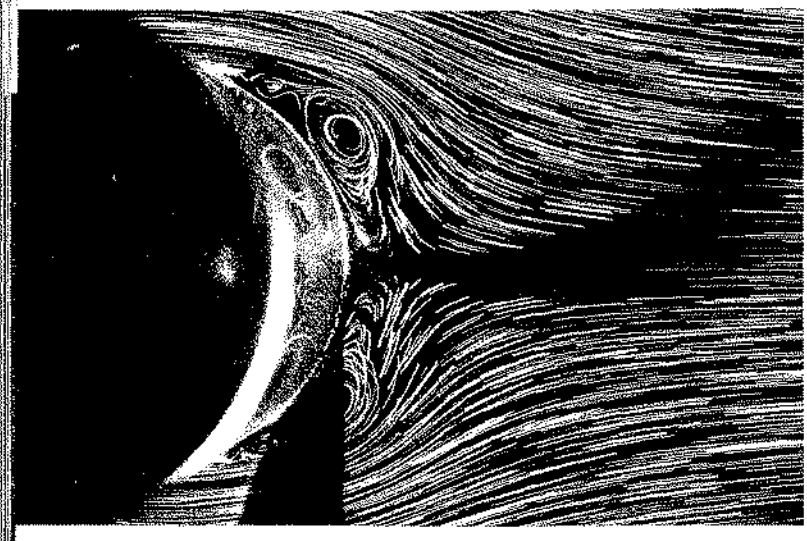

$R=5000,\ Ut/d=1.0$

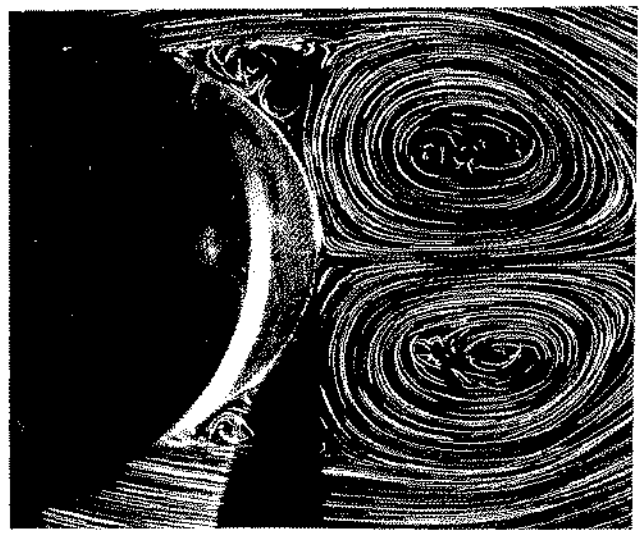

$R=5000,\ Ut/d=3.0$

59. Impulsive start of a circular cylinder. The camera moves with the cylinder, of which only the lighted rear surface is seen. The dark angle below results from a difference in refractive index of the Plexiglas cylinder and the oil through which it is set in motion. The tracer particles a fine magnesium cuttings. *Photograph by Madeleine Couta ceau and Roger Bouard*

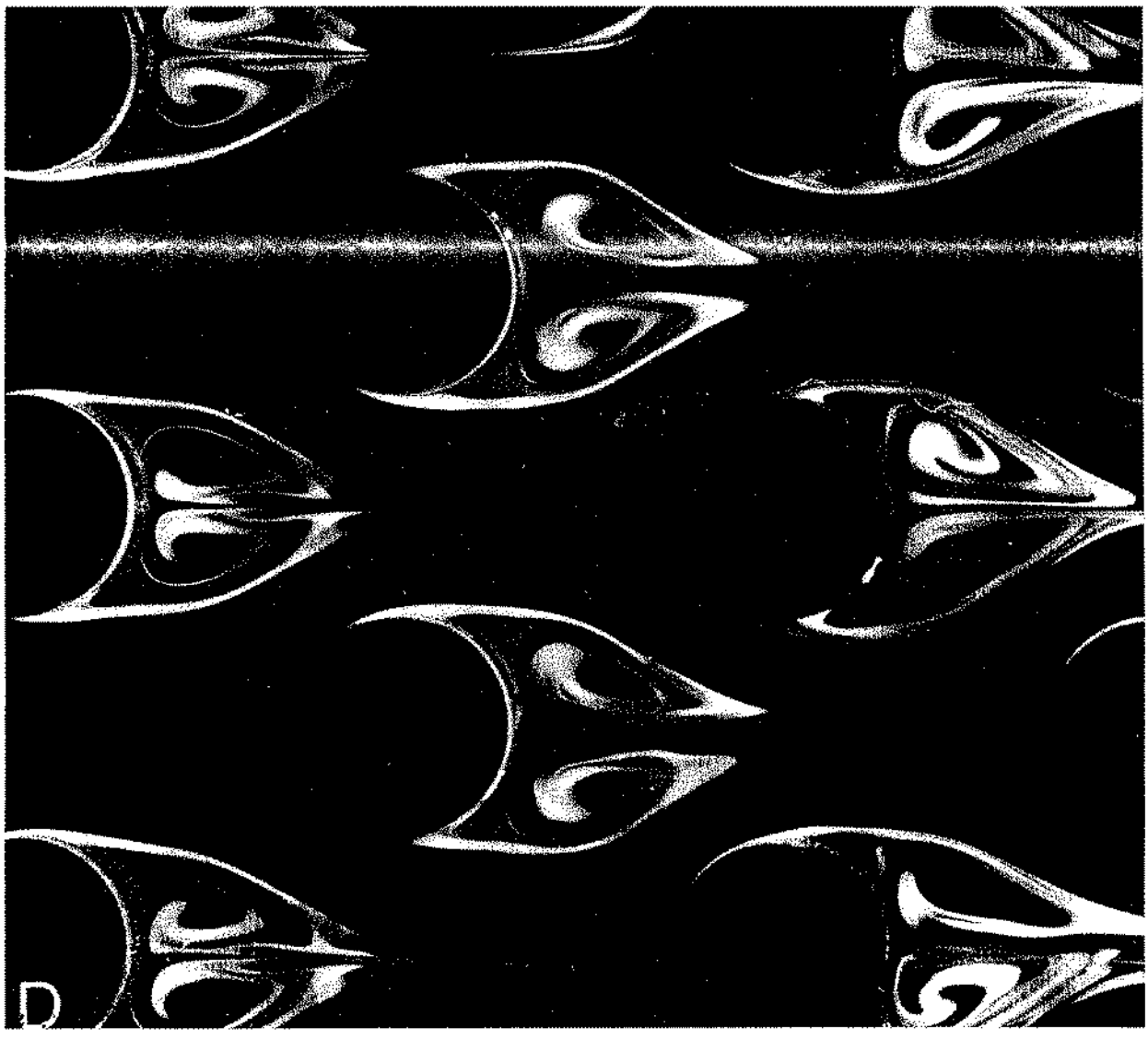

60. Impulsive start of a staggered array of circular cylinders. The Reynolds number is 3000 based on the diameter. The array has moved about ten diameters. *ONERA photograph, Werlé & Gallon 1973*

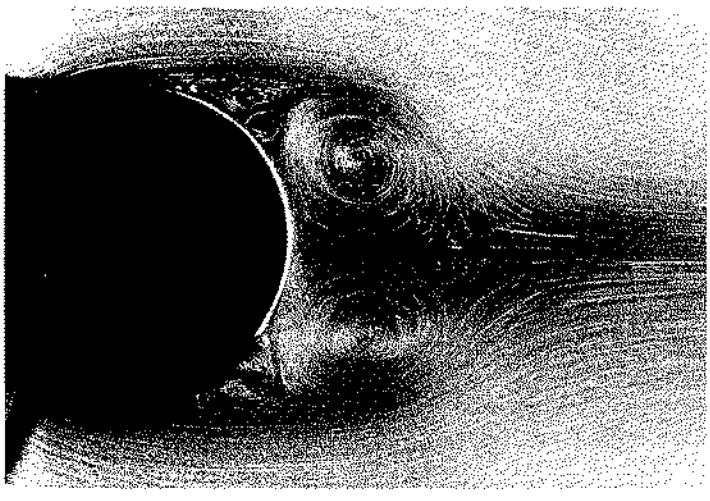

61. Impulsive start of a circular cylinder at R=1700, Ut/d=1.92. Aluminum dust in water gives a different view of the motion on the opposite page. It clearly shows the pair of small secondary vortices upstream of each main one. *Honji & Taneda 1969*

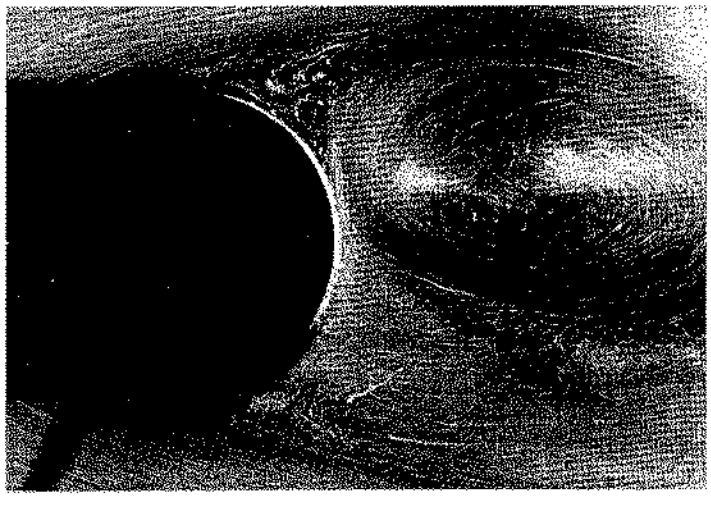

62. Impulsive start of a circular cylinder at R=1700, Ut/d=4.05. At this later stage the wake has lost its original symmetry, and is beginning to shed vortices into the stream. *Honji & Taneda 1969*

6. Turbulence

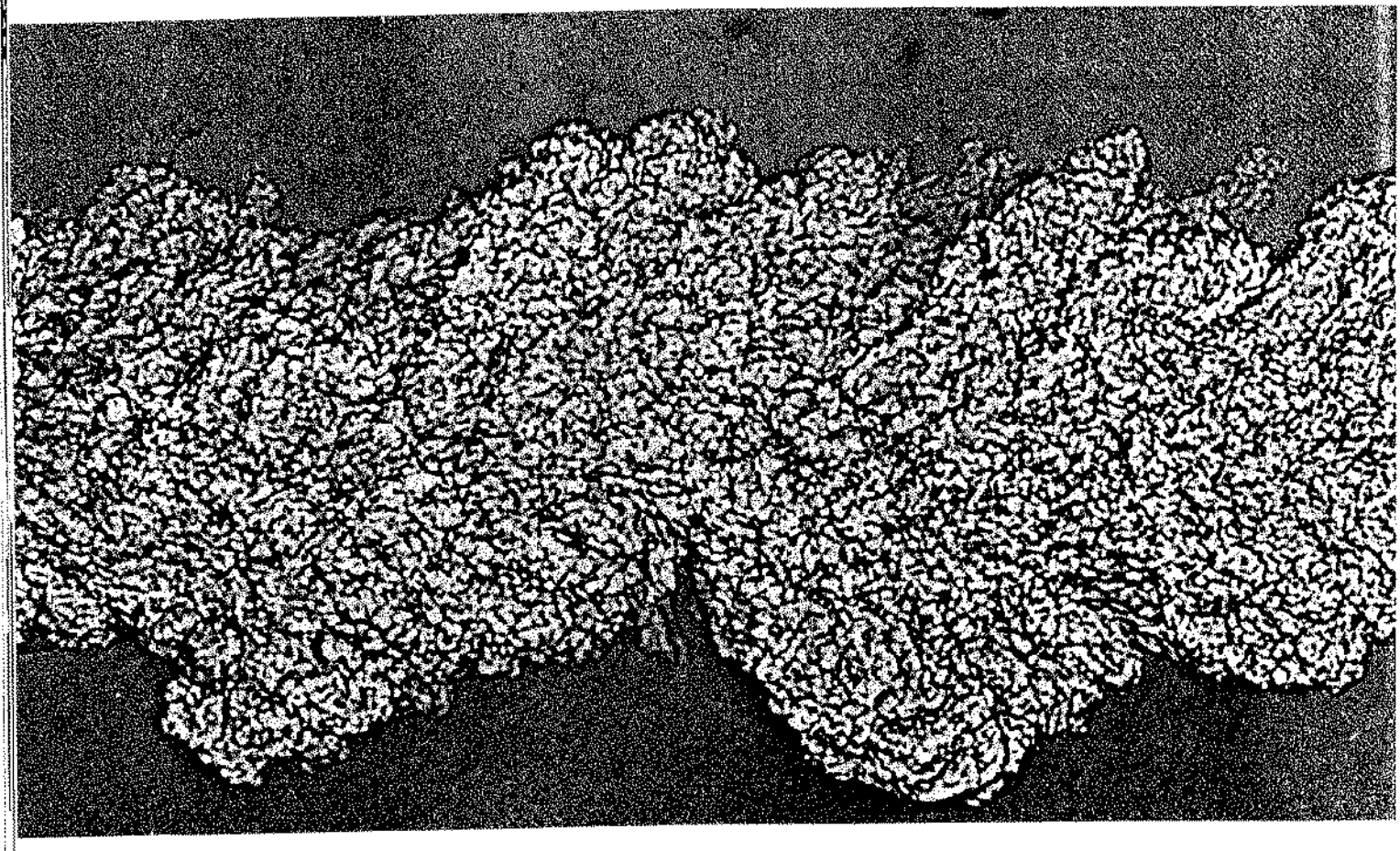

151. Turbulent wake far behind a projectile. A bullet has been shot through the atmosphere at supersonic speed, and is now several hundred wake diameters to the left. This short-duration shadowgraph shows the remarkable sharpness of the irregular boundary between the highly turbulent wake produced by the bullet and the almost quiescent air in irrotational motion outside. *Photograph made at Ballistic Research Laboratories, Aberdeen Proving Ground, in Corrsin & Kistler 1954*

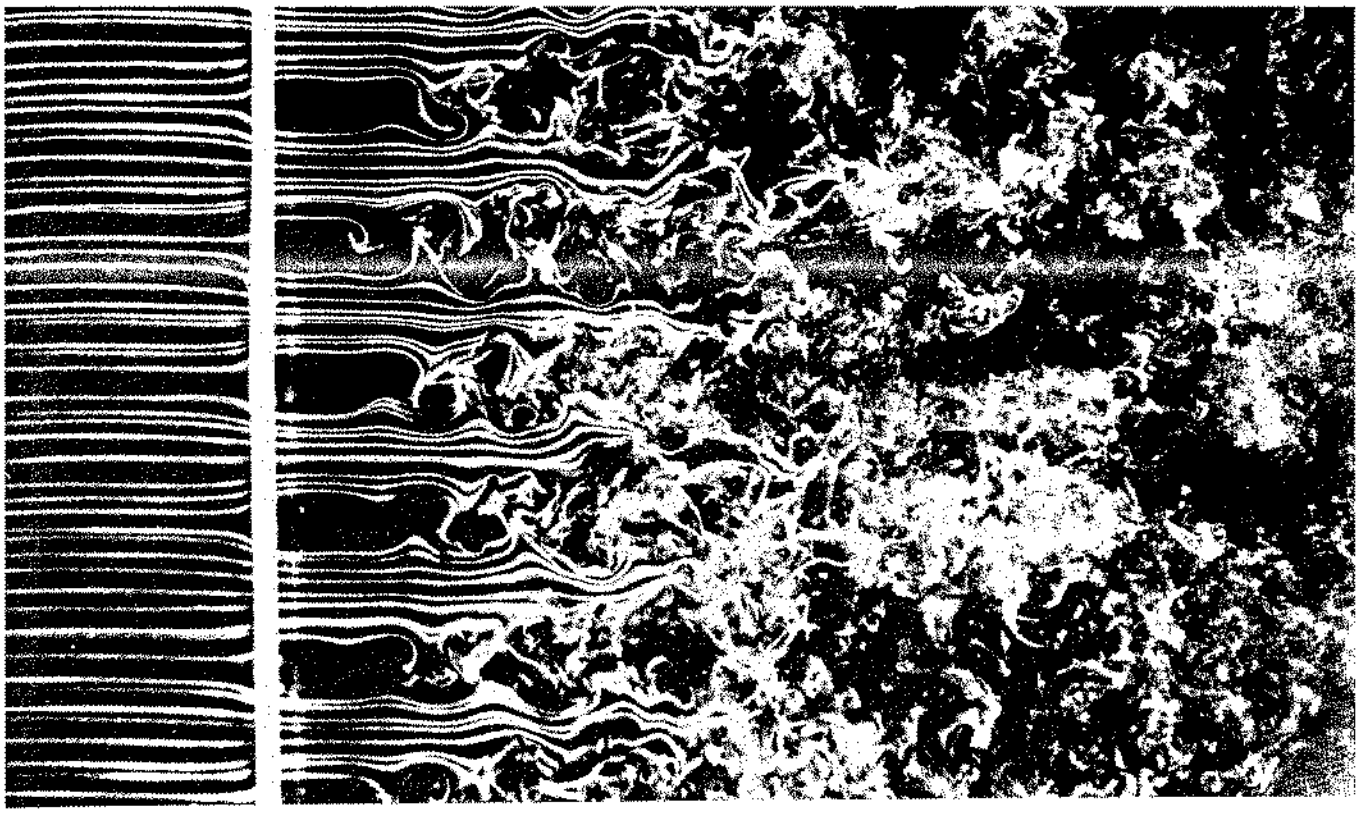

152. Generation of turbulence by a grid. Smoke wires show a uniform laminar stream passing through a $\frac{1}{16}$-inch plate with ¾-inch square perforations. The Reynolds number is 1500 based on the 1-inch mesh size. Instability of the shear layers leads to turbulent flow downstream. *Photograph by Thomas Corke and Hassan Nagib*

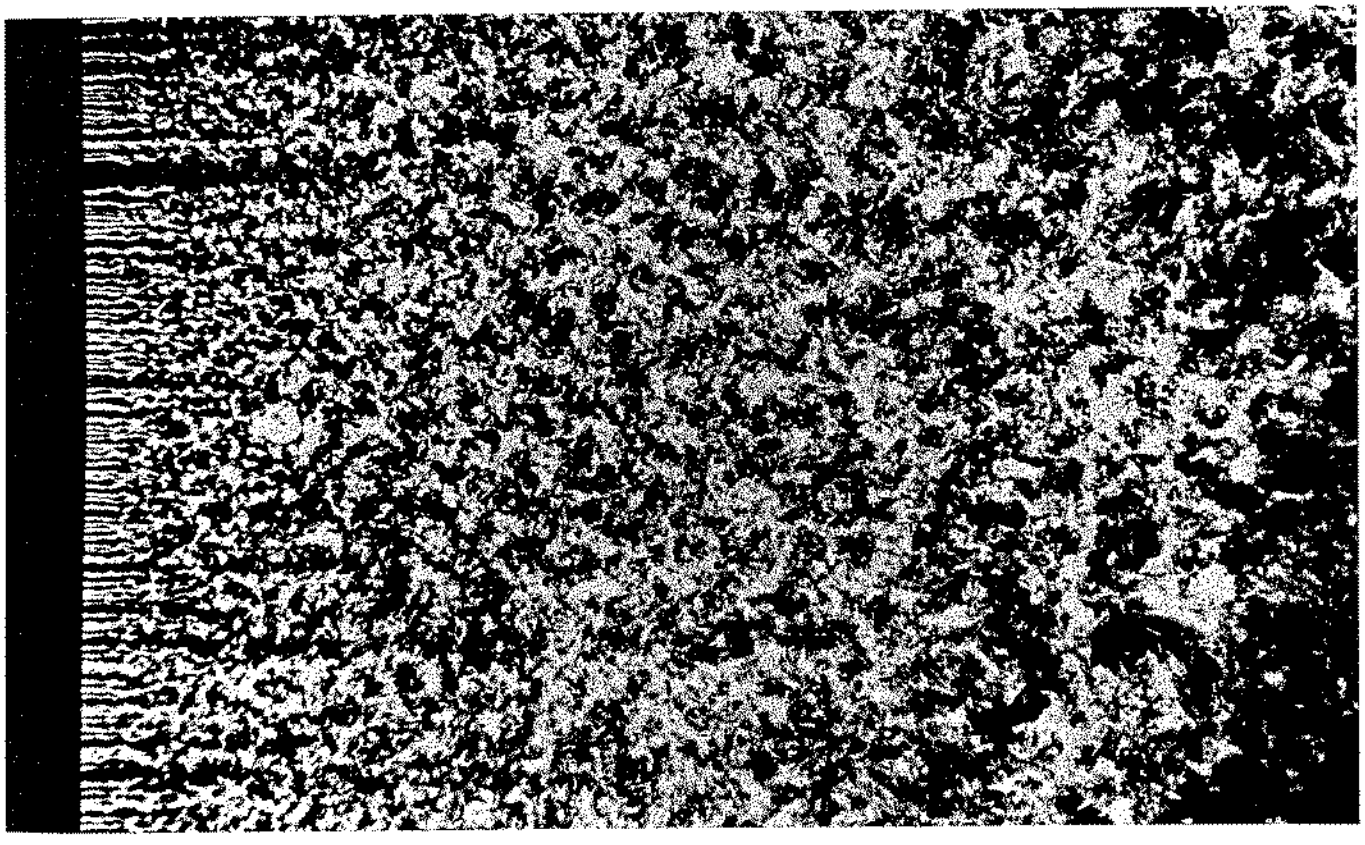

153. Homogeneous turbulence behind a grid. Behind a finer grid than above, the merging unstable wakes quickly form a homogeneous field. As it decays downstream, it provides a useful approximation to the idealization of isotropic turbulence. *Photograph by Thomas Corke and Hassan Nagib*

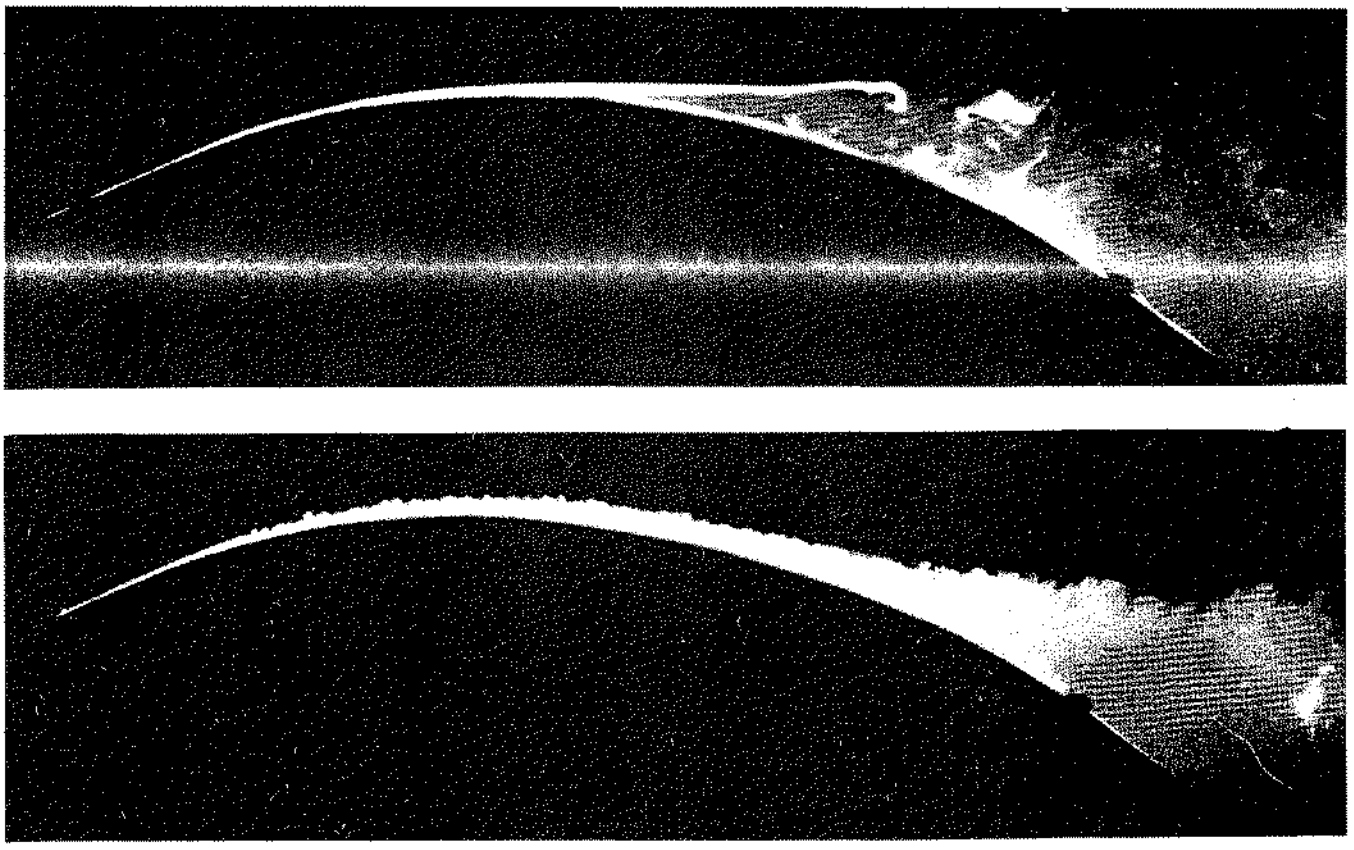

156. Comparison of laminar and turbulent boundary layers. The laminar boundary layer in the upper photograph separates from the crest of a convex surface (cf. figure 38), whereas the turbulent layer in the second photograph remains attached; similar behavior is shown below for a sharp corner. (Cf. figures 55-58 for a sphere.) Titanium tetrachloride is painted on the forepart of the model in a wind tunnel. *Head 1982*